POLITECNICO DI TORINO

Master's Degree in Mechanical Engineering

Modelling, Control and Testing Methodology of Hybrid Powertrains with Recycled Permanent Magnet-based Electric Machines

Supervisors

Prof. Angelo BONFITTO

Prof. Nicola AMATI

Candidate

Saulius PAKŠTYS

October 2022

Abstract

Due to the global rising concern regarding humanity's impact on the environment and the consequences that will arise from it, many engineering industries are moving towards a more sustainable level of production, material usage and system operation. Institutions and corporations have a common goal in uncovering novel solutions to mitigate this impact. Supporting this notion, the European Institute of Technology has proposed a project involving several partners in investigating the viability of utilizing recycled permanent magnets in permanent magnet synchronous motors (PMSMs) for application in the automotive industry, a sector that has an undeniable impact on the world's progression towards a more sustainable future. In addition, the project aims to decouple the EU from a dependency on natural resources necessary for NdFeB magnet production, the most efficient and widely implemented magnet type within PMSMs.

The following study is an interdisciplinary activity that follows the project from the Politecnico di Torino's involvement, mainly in evaluation of the virgin and recycled magnet motors at component and vehicle level. A formulation of a testing methodology that can be applied to virgin magnet (VM) machines as well as recycled magnet (RM) machines is discussed, where the exploration of various evaluation routes are presented. Particularly, the static and dynamic characterizations of the machines are separated into numerical and experimental routes, with the development of an Equivalent Consumption Minimization Strategy (ECMS) with temperature feedback for the vehicle control.

The structure of the thesis is guided by certain working points of the project, where firstly a state-of-the-art analysis on the various methods of magnet recycling and their viability is performed. It investigates the main solutions that are beginning to emerge, as well as their economic and environmental advantages and disadvantages in comparison to virgin magnet production. Following this, the numerical modelling and control of the P2 hybrid powertrain on MATLAB® and Simulink® is discussed, which is necessary for the dynamic characterization of the electric machines. Here, the conventional ECMS and temperature based ECMS

are presented, generating two routes from which an analyst may use to evaluate the performance of the selected machine implemented. Subsequently, the testing methodology is explored, where the static characterisation experimentation including the design of the mechanical interface for the testing assembly is presented. Here, the outline of the dynamic characterization is also discussed, experimentally and numerically.

Acknowledgements

I wish to express my deepest gratitude firstly to my brother Marius Pakštys, for the unwavering support he has given me over the time spent to obtain my Master degree. When moments became difficult and seemingly insuperable, he was there for me. Likewise I have shared successes with him that have contributed to my personal growth, and for all this I am grateful. My parents, who have supported me throughout my tertiary studies, can not be thanked enough. From the many visits my Dad made to help and support me while I study, to the long discussions with my Mom concerning life and aspirations, they have always been by my side. For all this, they deserve everything of the world. I wish to also thank my grandparents, for bringing me joy in reminiscing the sweet memories of my childhood and the positivity they project into my life.

I would like to thank my academic advisor, Professor Angelo Bonfitto, for the guidance, support and the vast number of opportunities he has offered me over the course of the thesis. His continuous advice and initiation of my involvement in parallel projects is deeply appreciated, as it has given me the opportunity to expand my knowledge beyond the scope of the degree for which I have studied. I have been able to pursue my passion for the automotive world, one that I have not been entirely true to since beginning my studies at the Politecnico. For this, I wish to thank both Professor Nicola Amati and my academic advisor for making it happen.

Finally I must thank my closest friends: Rodrigo, Luca, Gianluca, Carina, and Julia for the memorable moments we have shared with our time together. You have made my university life unforgettable, with the many laughs and conversations we have had with each other. When days became heavier, I knew you would lift my spirits and for this I hold you dear to me. I would also like to thank my dear friend Gaia, for her continued support and belief in me, even across borders. She has been on this journey with me from the beginning, and we have shared the highs and lows together from which she has helped me grow. I consider myself incredibly lucky to have met everyone and to call each one of you my friend, thank you.

Table of Contents

List of Tables

List of Figures

Chapter 1

Introduction

1.1 Project

The work presented herein closely follows the "Recycled Magnet-based Motor Digitalised Virtual Production Test Bed" (eVTB) project funded by the European Institute of Technology (EIT) and particularly that of the Politecnico di Torino's involvement. The aim of the project is to provide a set of tools for the redesign of electric machines (EMs) with recycled components for hybrid electric vehicles (HEV) and evaluate their performance. The foundation of the proposal and ultimately the commencing of the project lies within two core reasons. The first is the mitigation of waste and sustainable utilisation of materials for the production of new components, aiming to also limit the production of greenhouse gases that contribute to global temperature rise. The second is centered in the principle of self-reliance of the European Union, limiting its dependency on external nations for critical materials and components necessary to sustain its throughput and growth of various industries (ie automotive and energy).

The main concept of the project is to outfit an electric machine with magnets produced using virgin magnet (VM) material, characterise it fully and compare it with an identical machine outfitted with magnets produced from recycled magnet material (RM). This means evaluating its performance at component level, as well as at vehicle level, where in both cases the testing methodology is presented through a numerical and experimental approach. The dynamic evaluation of the machine's performance at system level includes its implementation on a P2 hybrid powertrain in a light duty vehicle (LDV). Due to the use of recycled material, a hypothesis may be made regarding the machine's performance: it will exhibit a lower efficiency as well as a lower peak torque production compared to the VM EM. This can be stated with reasonable certainty due to the introduction of impurities during the

recovery processes of end-of-life (EOL) magnet material. These processes will be explored in depth in Chapter 2 of this work.

The experimental testing of the EM takes place at the CARS center located in the main campus of the Politecnico di Torino, a newly built facility by AVL outfitted with the necessary equipment able to evaluate individual components and full vehicles. The three end-goals to be achieved from the static characterisation are:

1. Impedance characterisation - resistances and phase inductances (L_d and L_q).

2. Open circuit tests - cogging torque and k_e constant estimation.

3. Static measurement of the torque-speed characteristic and the efficiency map.

To carry out the testing of the machine effectively, the experimental set-up must be defined accordingly. This is performed with the aid of one of the partners of the project: Dayco. The company develops and manufacturers powertain solutions for automotive and industrial applications, particularly having a vast experience in testing of components and vehicle systems.

To characterise the machine dynamically with its implementation on a P2 hybrid architecture, a numerical model of the system that represents all the pertinent components is required. This is done on MATLAB® and Simulink®, with the aim to study the performance of the vehicle with VM and RM machines. In particular, the goal is to obtain the fuel consumption and ultimately the CO_2 emission of the vehicle with the different EMs implemented. The vehicle model and its control strategy are presented in Chapter 3, with the introduction to various HEV control strategies as well as a presentation of the most prevalent subsystems. In addition two controllers are discussed: The baseline Equivalent Consumption Minimization Strategy (ECMS) and a developed ECMS based on temperature feedback.

Chapter 4 presents a testing methodology that follows an experimental and numerical route for both the static and dynamic characterisations of the machines. It provides the tools a designer and analyst may use to evaluate the EMs thoroughly, at component and at vehicle level. Furthermore, the said chapter discusses the methodology for the numerical static evaluation that involves a software based on the finite element method to generate the necessary maps that characterise an electric machine. The design of the mechanical interface between the EM and the prime mover used to emulate the internal combustion engine (ICE) for the experimental static evaluation is also presented.

In addition to the technical work executed, the activity during the period over which it is performed consisted of meetings with the various partners of the project. These were essential for periodic updates from the side of all that are involved, as well as to solve technical issues related to the work packages. Presentations were a key tool to portray these updates and issues, in addition to reports that were drafted to be officially sent to EIT. In general, the activity requested a high level of partner interaction and communication to meet deadlines, both internal and external. This lead to the activity being more than a traditional one, where on top of the research work, there was a good portion of leading aspects of the work package assigned to the Politecnico.

Before the topics above are to be explored, this section sets forth the objective value of the activity, a presentation of the the various components and layouts of HEVs, and working principles of EM drives to ground the reader in the nature of the aspects to be discussed.

1.2 Importance

Stepping back from the project objectives, one must consider the greater picture regarding the development of HEVs and their subsystems. The transportation sector is composed of aviation, ships, railway, and road, where this last member consumes 73% of the total energy used by said sector as reported in [1]. ICE based vehicles are the main type found on the roads, and with that are responsible for 25% to 30% of the total greenhouse gas emission. Within Europe, passenger cars and light commercial vehicles are responsible for around 12% and 2.5% of total EU CO_2 emissions respectively. The concept of a HEV is not novel (in 1898 Ferdinand Porsche produced his first vehicle: the Lohner Electric Chaise), where it was the cost and performance of battery packs that limited its emergence into retail markets at an early stage. Their major development has been executed in recent decades, allowing automakers to bridge the gap between the power of the ICE and emission-free nature of the EM.

Furthermore, the incentive for HEV development is not just limited to moral considerations, however also legislative. However granted, the following regulations enforced stem from environmentally-conscious bases. On 1 January, the EU enforced the Regulation (EU) 2019/631, which outlines the CO_2 emission threshold targets for new passenger cars and vans applying from 2020, 2025 and 2030. Furthermore, it includes a mechanism to incentivise the adoption of low to zero emission vehicles.

The targets set for 2020-2024 (based on WLTP test procedure) are the following:

- Cars: 95 g CO_2/km
- Vans: 147 g CO_2/km

It is important to note that these values are based on EU fleet-wide targets that take into account the average mass of the manufacturer's new vehicles registered in a given year. As explained in [2], this suggests that original equipment manufacturers (OEM) producing heavier cars are allowed higher average emissions compared to those producing lighter cars. Regarding targets for 2025-2030, the numbers become even more restrictive by applying a 15% reduction to the starting values indicated above (becoming 80.75 g CO_2/km for cars and 124.95 g CO_2/km for vans). For 2030 onwards the values are reduced by 37.5% for cars and 31% for vans (becoming 59.375 g CO_2/km and 101.43 g CO_2/km respectively). The penalties for the exceedance of these targets within their respective time frames comes at a cost to the manufacturer. In particular the cost is set at 95€per g CO_2/km of target exceedance.

One of the larger incentives directed towards manufacturers regards the zero and low-emission vehicles (ZLEV) crediting system. A ZLEV is defined as a vehicle with emissions between 0 and 50 g CO_2/km. From 2025, the incentive allows for the alleviation of a manufacturer's specific emission target if its share of new ZLEVs within a given year exceeds 15% for cars and vans. From 2030 onwards, these values are increased to 35% and 30% for cars and vans respectively.

Presently, data reported [2] indicates that following the implementation of the regulation, average CO_2 emissions of new passenger cars registered in the EU have decreased by 12% in 2020 compared to the previous year. In addition, the share of electric vehicles has tripled. These are promising data indicating a positive trend towards decarbonisation and carbon neutrality which the EU have set a goal for: net-zero by 2050, with an intermediate target of at least 55% net reduction of greenhouse gases by 2030. With the strong focus on environmental considerations, the EU have imposed strict legislations that manufacturers must abide by that would ultimately lead to a lower diffusion of greenhouse gases as well as promoting gross domestic product increases and employment opportunities.

1.3 HEV drives

Considering the project at hand, the factors for identifying the machine typology to be tested must be addressed. There are a number of solutions automakers can turn to regarding electric drives (their fundamental requirement being to generate

torque) such as direct current (DC), induction, or synchronous machines. A brief overview of the existing technologies is necessary in order to motivate the particular machine type selected in this project.

1.3.1 Machine types

DC machines depend on the use of a direct excitation current that induces a magnetic field which interacts with the field generated in the rotor due to the armature current, generating torque. Permanent magnets in the stator are also used in some designs to produce the magnetic field excitation. Two types of topologies are available: brushed and brushless (BLDC). The latter is the result of reversing the position of the stator and rotor of a permanent magnet DC machine, displaying high efficiency, compactness and high energy density [1]. The former was the initial choice for electric vehicles (EVs), however has since been replaced due to their lower efficiency, power density, and maintenance issues. BLDCs are typically implemented in two-wheeler applications as in-wheel solutions, as well as in electric vehicle conversion kits.

Induction machines (IM) use a three phase alternating current (as a minimum) in the stator that induces a current in the windings of the rotor and therefore generating the required torque. They are simple in their construction, with two main solutions existing: wound and squirrel-cage. The former is less attractive for automotive applications due to higher cost and maintenance requirements, however both designs exhibit good reliability and ability to operate in hostile environments [3]. The machine typology can be seen in Figure 1.1

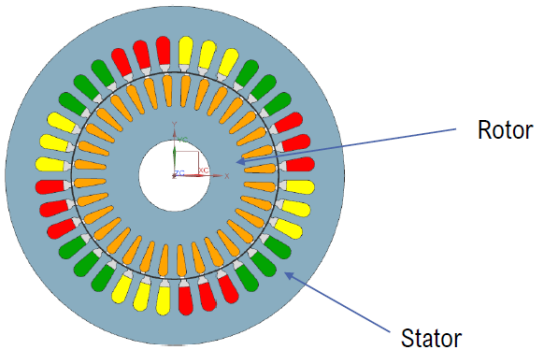

Figure 1.1: Induction machine

Synchronous machines operate similarly to IMs, however the rotation of

the rotor is synchronised with the frequency of the AC current. Two main types are employed in drivetrain technologies: permanent magnet (PMSM) and switch reluctance (SRM) machines. The former depends on rare-earth magnets to increase the flux density in the air gap while the latter operates on the principle of variable reluctance. SRMs display a high mechanical integrity, thus are suitable for in-wheel drive systems. Furthermore, with rapid acceleration and high-speed operation capabilities, they are advantageous in gear-less EV propulsion. However SRMs exhibit low torque density, high torque ripple and high acoustic noise. PMSMs are less noisy, are more reliable and display a high performance across a wide speed range. These machines are also easy to control due to lower rotor inertia, are smaller in size and are able to be cooled more effectively. With these appealing features, PMSMs are the preferred choice in EV drivetrains, and therefore are the machine typology of choice for the eVTB project. A cross-section of the machine structure is seen in Figure 1.2.

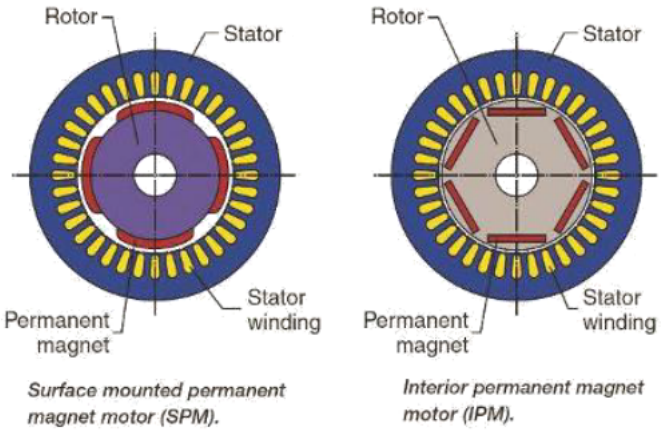

Figure 1.2: Surface and Interior mounted PMSM

As can be seen in Table 1.1 that is reported in [3], IMs display a lower efficiency and power density compared to PMSMs. However this does not mean they are entirely disregarded as they display a simple design with good control and low cost. The demerit of SR machines is their high acoustic noise and lower efficiency, while DC machines fall behind in most categories with respect to the other typologies. In general, the choice is often between an IM or PMSM, with BLDCs being appealing for a narrower gap of application (two-wheelers).

Since PMSMs are widely utilised in industry and are produced using magnet materials that are mined exclusively in certain regions of the planet (discussed

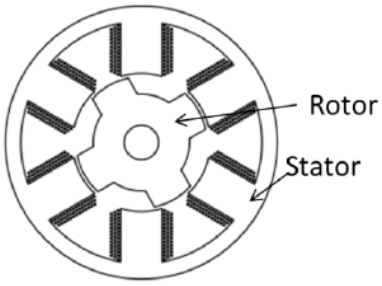

Figure 1.3: Switch reluctance machine

further in Chapter 2), the PMSM makes an ideal candidate to be studied within the project. It exhibits great potential for sustainable design and therefore merits the efforts of its experimentation as anticipted in this chapter. To understand the parameters that are required to be extracted from the machine, one must study the physics that describe such a device, outlined in the following subsection.

Factors	DC	Induction	SRM	PMSM	PM BLDC
Power Density	2	3	3.5	4.5	5
Efficiency	2	3	3.5	4.5	5
Controllability	5	4	3	4	4
Reliability	3	5	5	4	4
Maturity	5	5	4	5	4
Cost level	4	5	4	3	3
Noise level	3	5	2	5	5
Maintenance	1	5	5	5	5
Total	25	35	30	35	35

Table 1.1: Summary of main features of EV drives (1: worst, 5: best) after Karki et. al., 2020

1.3.2 PMSM operating principles

The Interior PMSM is a synchronous machine that uses permanent magnets built into the rotor as opposed to its close relative, the Surface PMSM where the magnets are mounted on the surface of the rotor. Generally it finds applications due to three main reasons:

1. Axial flux concentration.

2. Structural strength - the rotor is able to rotate at higher speeds.

3. The machine is able to be driven over a wide speed range through the use of field weakening control.

A synchronous machine displays features of a DC and induction machine. The stator is similar to that of an induction EM, while the difference lies in the rotor where the windings are normally connected via slip rings or other means to a source of direct current. The operating principle is as follows: the stator current produces a rotating magnetic field while the direct current in a p-pole field winding in the rotor generates a magnetic field rotating at rotor speed. If the rotor speed matches the stator field speed and there is no load torque, the two fields align. However if there is a load torque present, there will be a delay of a some degrees between the two fields which develops torque. As the load increases the torque increases, where the maximum value is seen when the rotor field lags the stator field by 90 degrees. Regarding a PMSM, the rotor field is generated through the permanent magnets present rather than the direct current as observed in a regular synchronous machine. Due to the absence of Joule losses in the rotor, the machine is more efficient compared to an IM, finding applications in variable speed drives.

With the core operating concept of the machine outlined, the governing equations of the machine must be addressed. The dynamic relation can be given by the following equation written in the three phase temporal system:

$$\boldsymbol{v_{abc}} = \frac{d}{dt}\boldsymbol{\lambda_{abc}} + \boldsymbol{R_{abc}}\boldsymbol{i_{abc}} \tag{1.1}$$

where v_{abc} (A.1) is the vector of voltages in the directions a,b and c, while λ_{abc} is the vector of flux linkages represented by the following equation:

$$\boldsymbol{\lambda_{abc}} = \boldsymbol{L_{abc}}\boldsymbol{i_{abc}} + \boldsymbol{\lambda_{p,abc}} \tag{1.2}$$

R_{abc} (A.5) denotes the matrix of resistances and i_{abc} (A.2) the vector of currents. L_{abc} (A.3) and $\lambda_{p,abc}$ (A.4) refer to the matrix of inductances (comprised of auto and mutual-inductances) and the vector of permanent flux linkages respectively. The latter contains entries in terms of the electrical angle θ_e and the permanent flux linkage defined through the following expression:

$$\lambda_p = N\Phi_p \tag{1.3}$$

where Φ_p is the magnetic flux and N the number of turns of the conductor. It is important to note that the flux of a magnet is directly correlated to the remanent magnetic flux density $B_r = \mu_r H_c$ through the known expression:

$$\Phi_p = B_r \cdot A\cos(\theta) \tag{1.4}$$

where θ is the angle with the vector to which the magnetic flux is perpendicular to, and A is the area of the magnet. It is evident that the permanent flux linkage of the machine is highly dependent on the magnets used, where if there is a degradation of the relevant parameters one observes performance limitations of the EM.

One issue with the current machine equations is that they are in the three phase temporal system, in a manner that is more difficult to deal with. Therefore the Park and Clarke transforms are implemented to simplify the calculations of the current and voltage waveforms in AC to DC. The Clarke transform ($\boldsymbol{T_c}$) converts the system from a three phase variable (abc) to a stationary orthogonal representation ($\alpha\beta$). The Park transform ($\boldsymbol{T_p}$) converts the two-phase stationary frame of reference (fixed to the stator) to a rotating reference frame (dq) fixed to the rotor. It must be noted that the d-axis is aligned with the poles of the magnet, while the q-axis is aligned with the gaps. One may obtain a final Park-Clarke transformation matrix ($\boldsymbol{T_{pc}}$) by simply performing the product between the two. The Clarke, Park and Park-Clarke matrices are reported in Appendix A, in sections A.6, A.7, and A.8 respectively. Figure 1.4 provides graphical support to the statements made.

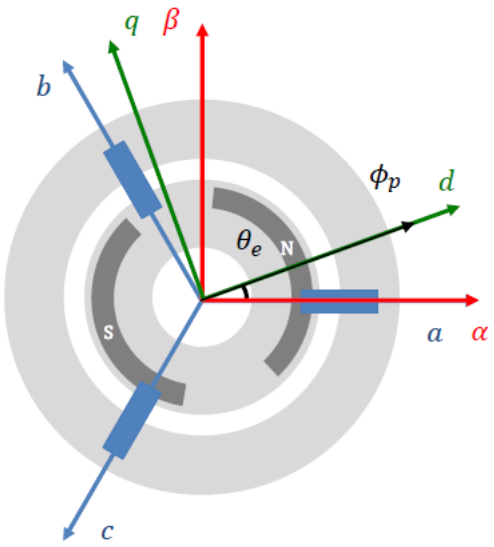

Figure 1.4: Reference frames of the machine

Applying the Park-Clarke transform to the dynamic relation of the machine, one obtains the following expression:

$$\boldsymbol{v_{dq}} = \boldsymbol{T_{pc}}\frac{d}{dt}(\boldsymbol{L_{abc}}\boldsymbol{T_{pc}^{-1}}\boldsymbol{i_{abc}} + \boldsymbol{\lambda_{p,abc}}) + \boldsymbol{T_{pc}}\boldsymbol{R_{abc}}\boldsymbol{T_{pc}^{-1}}\boldsymbol{i_{abc}} \tag{1.5}$$

Given that the electrical angle is defined as follows:

$$\theta_e = pt\Omega \tag{1.6}$$

where Ω and p are the mechanical angular speed of the rotor and pole pair number respectively, and by working on the dynamic equation in the rotating frame of reference, one obtains the following expressions for the direct and quadrature voltages:

$$v_d = L_d \frac{di_d}{dt} - L_q i_q \Omega_e + R i_d \tag{1.7}$$

$$v_q = L_q \frac{di_q}{dt} - L_d i_d \Omega_e + \lambda_p \Omega_e + R i_q \tag{1.8}$$

Furthermore, the direct and quadrature inductances are extracted from Equation 1.5 and are given as:

$$L_d = \frac{3}{2}(L_1 - L_2) \tag{1.9}$$

$$L_q = \frac{3}{2}(L_1 + L_2) \tag{1.10}$$

With the various terms defined, the expressions for the power and torque of the machine may be addressed. Firstly, the power is expressed simply as the combination of direct and quadrature power values, namely $v_d i_d$ and $v_q i_q$. When the expressions are subtituted in, one obtains:

$$P = \frac{3}{2}\left(L_d i_d \frac{di_d}{dt} + L_q i_q \frac{di_q}{dt} + p(L_d - L_q) i_d i_q \Omega + p i_q \lambda \Omega + R(i_d^2 + i_q^2)\right) \tag{1.11}$$

The time dependent terms give us an understanding of the variation of magnetic energy of the machine, while the terms with the pole pair number define the air-gap power that is associated to the mechanical power. The term with the phase resistance of the conductors indicates the Joule losses.

The torque is defined in terms of the power, particularly through the well-known relation: $P_{ag} = T\Omega$, where only the air gap and Joule loss power terms are considered. Through the substitution of the expressions of the associated terms, the final expression for the torque is defined to be:

$$T = \frac{3}{2} p i_q \lambda_p + \frac{3}{2} p (L_d - L_q) i_d i_q \tag{1.12}$$

It can be noted that the first term of the equation is the permanent magnet alignment torque, while the second term is the reluctance torque. When considering the torque-speed relation, it can be seen that with the mechanical speed increasing to infinity, the torque reduces to null. In reality an infinite value is not feasible, and

therefore by increasing it to a substantially large value, the maximum mechanical speed of the machine is obtained (Ω_{max}). The behaviour of the torque with respect to the mechanical speed of the machine is evident in Figure 1.5. The area before the base speed is known as the constant-torque region, while after this discriminant value is the constant power region. The torque-speed map characteristic, along with the efficiency map are the identity cards of any EM, providing information on the output given certain operating conditions. These graphs form the representation of the EM within the modelling stages of the project, and shall be introduced in Chapter 3.

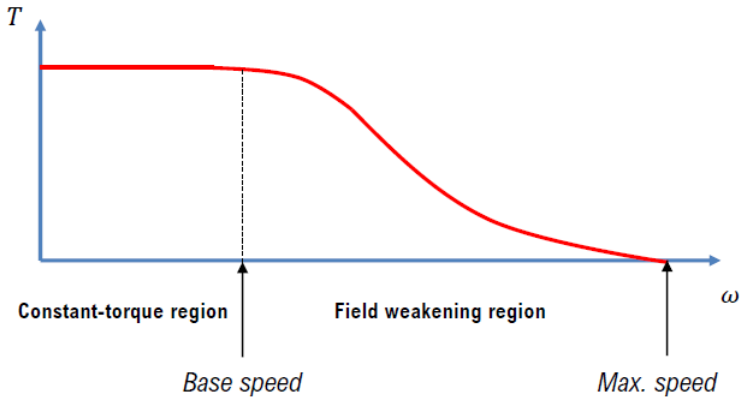

Figure 1.5: Torque-speed characteristic of a PMSM

1.4 Electric Machine

The machine for this project is supplied by a company named Physis which concerns itself with the manufacture and development of electric machines directed towards automotive and industrial applications. The machine is classed as high voltage (345.6 V) and displays a concentrated winding of the copper. It is an Interior PMSM that utilises Neodymium-Iron-Boron (NdFeB) magnets embedded in the rotor and has a nominal power of 48.6 kW. Additional parameters of the machine are seen in Table 1.2, while a view of the EM and its rotor are visible in Figure 1.6.

Regarding material specifications, the rotor and the stator are both manufactured from electrical steel with the former laminated with 0.3 mm sheets, while the latter is laminated with 0.35 mm sheets. The virgin magnets implemented are of the type N40UH. The conductor is made from copper and the cooling jacket is manufactured

from aluminium, with water-glycol as the circulating coolant. It is requested to have the coolant at 65°C, set at a flow rate of 6.4 liters per minute.

Parameter	Value
Filling factor	0.68
Pole pair number	10
Phase resistance [mΩ]	11
Peak torque [Nm]	330
Continuous torque [Nm]	100
Maximum copper temperature [°C]	150
Efficiency [%]	96

Table 1.2: Main features of the Physis Machine

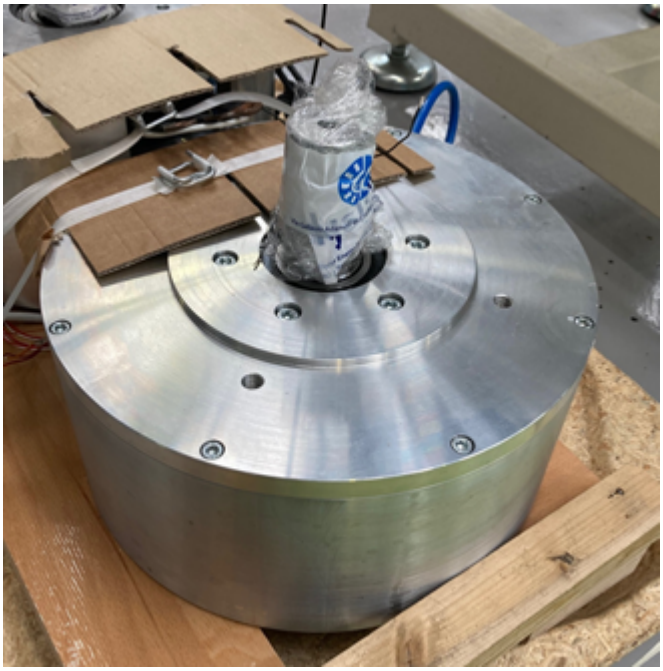

Figure 1.6: Physis 48.6 kW electric machine

1.5 Accompanying HEV powertrain components

Having presented the machine for the project, the reasoning for its choice and the governing physics, the additional components present within a HEV should be briefly introduced due to their important role in the vehicle's operation.

Beginning with the **bidirectional AC/DC converter (inverter)**, this component is essential for the conversion of direct current (DC) to three-phase alternating current required by the EM. It also works in the reverse direction, supplying DC to the energy storage system. Various topologies of traction inverters exist, namely voltage source (VSI), current source inverter (CSI), and impedence source (ZSI) inverters. The CSI may be used for speed control of AC machines, mainly induction machines with varying load torque, while the VSI offers more advantages such as being able to to be used practically for single-phase and three-phase applications. The latter exhibits a good speed range, simple regulator design and multiple motor controls from a single unit, however it also induces harmonics, cogging and jerky start and stop motions. Finally, the ZSI is the most promising of the three for HEV applications due to its higher efficiency and drive system reliability. It displays a Z network connected to the well-established inverter bridge, and is able to provide AC voltages regardless of the input voltage.

The **hybrid energy storage system (HESS)** is a crucial link in the energy flow of a HEV, where its composition based on the latest trends as seen in [1] consists of a battery and an ultracapacitor (UC). In the pairing of the two substituents, the battery is present to fulfill the low-frequency requirements, while the UC is able to provide high frequency and high magnitude power. Batteries are typically Lithium-ion based and in general have a low cost per watt hour, high energy density, however a short life cycle and low specific power. Batteries may be integrated into HEVs on three different levels: as cells, modules (comprised of cells) or battery packs (comprised of modules) which are typically found in modern HEVs. On the other hand, UCs display a long life cycle (quasi-infinite), ability to sustain highly dynamic power profiles, low energy density and a high cost per watt hour. The combination of the two components leads to a stability of the HESS, as the sudden load variations are absorbed by the UC while the battery is in operation, maintaining the DC-bus voltage. The battery conversely maintains the SOC of the UC. Regarding this operational layout, the efficient use of batteries may be achieved (up to 90%), increasing their life cycle (due lower demand of high discharge rates). Typically, batteries are modelled with a resistance capacitor and several branches of resistors, and by adding an UC one produces a HESS. Figure 1.7 from [4] displays an example of such a storage system (in particular a passive cascaded type) for HEVs.

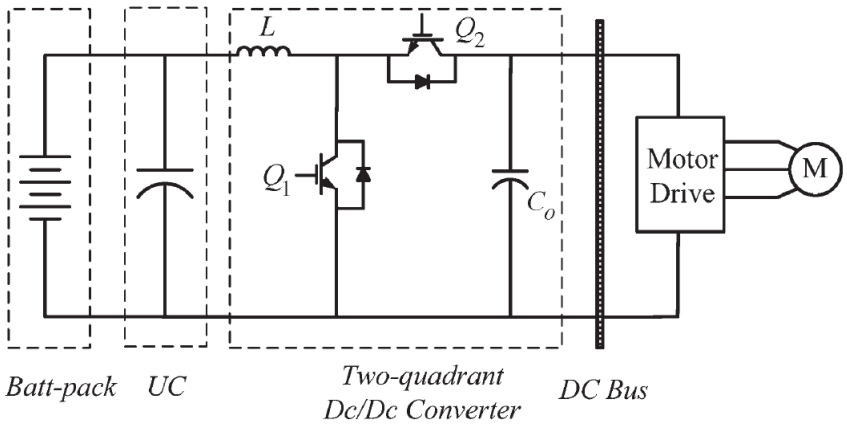

Figure 1.7: Passive cascaded UC/battery system for HEVs, after Khaligh et al., 2010

A **DC-DC converter** is another essential component present on a HEV powertrain, with unidirectional and bidirectional variants existing. The former type is responsible for supplying the auxiliary load, such as sensors, entertainment, and control equipment while the latter type is used during regenerative breaking, backup power and battery charging. Bidirectional converters exhibit two modes of operation: the first being *boost*, which refers to the power flow from the low voltage to the high voltage end, while the second is called *buck*, where the power flows from the high voltage to the low voltage end (battery recharging). The typology of the converter can further be broken down into isolated or non-isolated as reported in [5].

1.6 HEV architectures

With the most prominent components having been briefly introduced, the various hybrid electric vehicle layouts must be investigated. The three main types that currently exist are: series, parallel and series-parallel, labels that are associated with the energy flow within the system. Each offer their own set of advantages and disadvantages, with the parallel hybrid configuration being the most widly adopted due to compromises between cost and performance. Furthermore, three more general typolgies of hybrids exist which fall under the parallel hybird term: mild, full and plug-in (PHEV). These terms are associated with the performance of the EM integrated onto the powertrain.

As the name suggests, a **mild hybrid** system typically only provides a boost to

the ICE and is unable to propel the vehicle on electric power alone. For example it may be employed when the vehicle accelerates from a dead-stop or provides power to onboard systems such as air-conditioning. Normally found in the form of 48 V systems, mild hybrids do not need to be plugged in to recharge the battery, rather the charge is sustained through a combination of ICE power and regenerative breaking. The size of the machines typically installed range from 10 kW to 21 kW, able to generate a peak torque between 34 and 50 Nm [6].

Full hybrids are capable of propelling the vehicle with the EM alone over a significant distance, typically at lower city speeds. They recharge their battery in the same manner as mild hybrids. **PHEVs** are similar to full hybrids in their core concept however they offer the ability to recharge the battery through the grid. They thus have the largest electric-only range and often serve as a half-way point between full hybrid and full electric vehicles. Typically PHEVs begin operation in charge depletion mode (CD), and as soon as the state of charge of the battery reaches a threshold value, they begin operating in charge sustaining (CS) mode until the vehicle is parked and recharged.

1.6.1 Series

The main concept of this layout is a decoupling of the ICE with the driveline, where it is solely used to generate power that is stored in the battery. The EM draws upon this power and propels the vehicle. This can be clearly seen in Figure 1.8 from [1]. The advantages of this architecture are that the ICE is forced to operate in its narrow high efficiency region consistently, and the elimination of a multigear transmission due to the EM. However it also presents some disadvantages, namely that two EMs are required, and there are larger energy losses due to more energy conversions (mechanical to electrical through the generator and then vice versa through the motor). Generally it is implemented on heavy vehicles such as buses, trucks and military vehicles, however may also be seen in light commercial vehicles.

1.6.2 Parallel

As opposed to the series layout, traction power may be supplied by only the ICE, EM or both in the parallel configuration. With its greater operation versatility, it is the more readily adopted topology for light commercial vehicles. Parallel systems may be implemented as mild or full hybrid by varying the machine that is incorporated, being either low voltage (48 V) or high voltage (HV).

The parallel hybrid layout seen in Figure 1.9 from [1], allows for a versatility

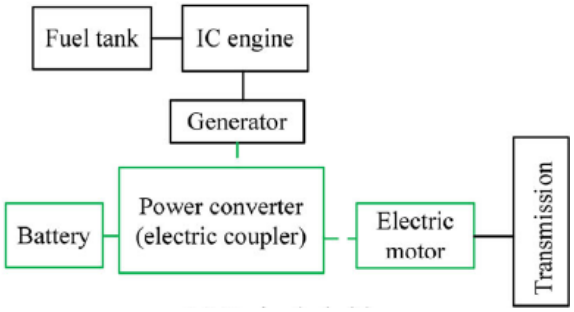

Figure 1.8: Series hybrid layout, after Singh et al., 2019

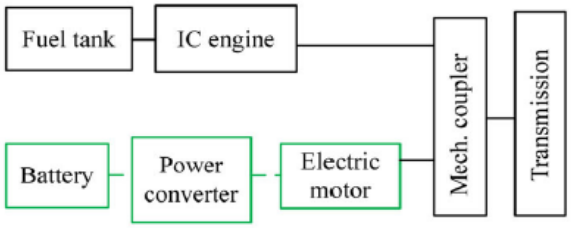

Figure 1.9: Parallel hybrid layout, after Singh et al., 2019

of the EM placement on the drivetrain, offering various supporting roles to the ICE. The different configurations are listed below and are visualised in Figure 1.10 extracted from [7]:

1. P0: Also called the 'belt starter generator' layout, the position of the machine is found at the front of the ICE, connected to the engine by means of a belt. This configuration offers the most cost effective way to electrify a vehicle due to its limited impact on the existing drivetrain layout. However, because the EM and the ICE are linked through the belt, they are unable to be separated and therefore the engine friction torque becomes a loss for the EM when it is engaged.

2. P1: Here the EM is directly connected to the crankshaft of the ICE, located before the clutch. The EM functions as a starter, generator and assisting motor, able to provide higher torque compared to the P0 configuration due to the absence of slip that is present with a belt connection. However as with the P0, the generator mode is affected by the ICE friction.

3. P2: The EM is attached to the driveline after the clutch by means of a belt or directly on the axis of the drive. The main advantage of this layout is the greater energy recuperation potential it presents, as the EM is able to be

disconnected from the ICE and therefore the friction losses no longer pose an issue. The disadvantage is that it has a higher cost of integration into the powertrain.

4. P3: In this configuration, the EM is placed on the transmission, particularly on the output shaft. It offers an even higher energy recuperation potential compared to the P2 layout as the engine and transmission friction losses are absent.

5. P4: The EM is completely disconnected from the ICE, where it drives the rear axle while the ICE drives the front axle. In some cases the machine is mounted in the wheel hubs and offers the possibility to have a four-wheel drive capability.

The discussed configurations are illustrated in Figure 1.10.

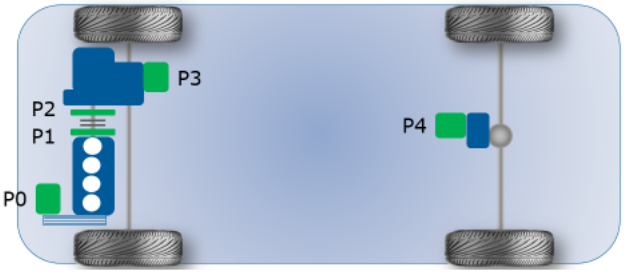

Figure 1.10: Various EM configurations

1.6.3 Series-parallel

Finally, a brief outline of this layout can be made. As the name suggests, it is a combination of the two previously discussed configurations, where a generator is added to a parallel layout. The power directed towards the battery thus arrives from two points: the ICE through the generator, and the EM connected to the driveline. Figure 1.11 from [1] depicts this energy flow. This layout allows for engine-only or EM-only operations, allowing for the ICE to run at near optimum efficiency for the majority of the time. Particularly, the series configuration is favoured at lower vehicle speeds where it is most efficient, while the parallel layout is utilised at higher speeds. The drawbacks of a series-parallel driveline are the higher costs it incurs compared to a pure parallel hybrid, as it requires a generator, larger battery pack and more computing power to control the dual system.

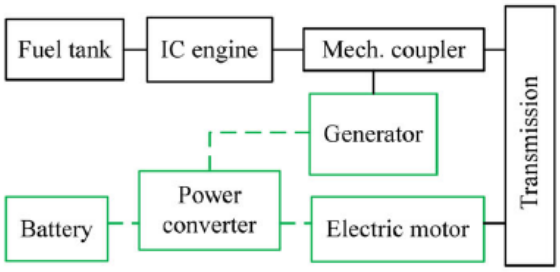

Figure 1.11: Series-parallel hybrid layout, after Singh et al., 2019

Chapter 2

Recycling Potential of NdFeB Material

2.1 Permanent magnet material and usage

Neodymium-iron-boron (NdFeB) magnets are, as of yet, the best performing magnets due to their high energy product (BH). PMSMs used within electric vehicles (EV) and HEVs are thus able to be realized in smaller dimensions producing the design torque required. Therefore, it is no surprise that sintered magnets account for approximately 92-95% of current NdFeB production by mass. Furthermore, NdFeB magnet EMs exhibit a lower environmental impact as compared to that of ferrite magnet motors for example, the latter displaying lower efficiencies and larger sizes.

These magnets are produced using rare earth elements (REE) such as neodymium (Nd) and praseodymium (Pr) which are considered as light rare earth elements (LREE). In addition, heavy rare earth elements (HREE) such as dysprosium (Dy) and terbium (Tb) are used. The REE of note considering automotive applications is Dy, as this element is added to the magnet to increase high temperature resistance: the motor is thus able to operate at elevated temperatures. However, one of the many issues concerning REEs is that Dy and Nd for example are expensive and by proxy so are the magnets, where around 70% of the motor cost is due to the magnet cost [8]. This ultimately does not deter manufacturers from using REEs for a wide range of applications as can be seen in Figure 2.1, namely in motors and generators for industrial applications (34.4%).

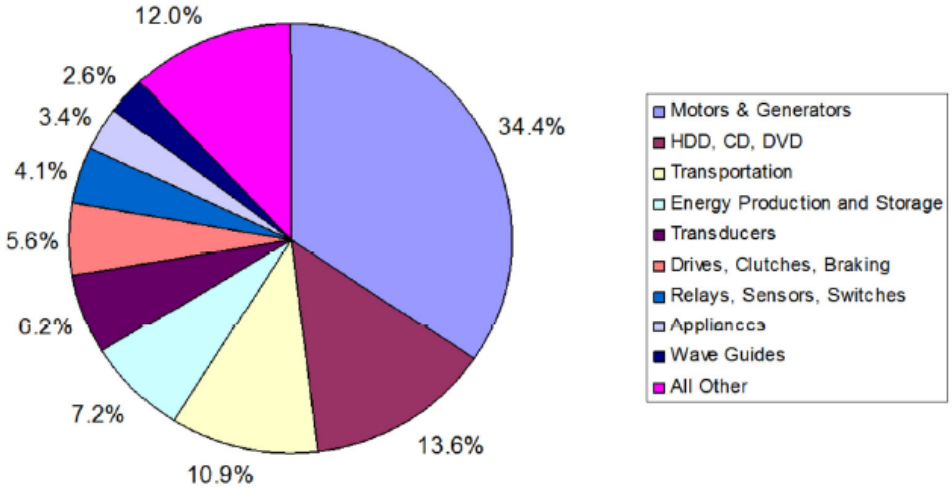

Figure 2.1: Share Usage of NdFeB Magnets in 2017, after Yang et al., 2016

2.2 Incentives for recycling

At present [9], less than 1% of REEs are recycled due to a lack of incentives, inefficient collection, and technological difficulties. As of yet, no concrete commercial procedure has been developed for the recycling of EOL permanent magnets, at least within the EU (Okon Metals Recycling and REECycle seem to be established entities in the United States). So far it is cheaper to buy REE master alloys or newly manufactured magnets rather than reprocess the complex scrap material from recycled sources. These sources include consumer electronics (hard disk drives), REE motors used in air-conditioning units, wind turbine generators, magnetic resonance imaging machines (MRI) and motors used in the transport industry (automotive and two-wheelers) as well as in industrial applications. This list is in line with what The European Rare Earths Competency Network (ERECON) has proposed as a list of priority products for which NdFeB recycling is most likely to become economically viable.

Considering this, one must examine incentives for recycling NdFeB magnets. Firstly, global in-use stocks of four REEs (Nd, Pr, Tb and Dy) amount to a total of 97 kt: a value which is four times the 2007 extraction rate of the individual elements. This introduces the concept of an 'urban mine', one that contains an immense potential for material as a secondary source, however, is yet to be tapped into. A material flow analysis of REEs in Europe by [10] shows that in 2010, 1230 tons of Nd flowed into the EU for magnet production, of which 507 tons has been reported into the waste stream with zero recycling. This may be a consequence of the methods

used for treatment of electronic waste: generally hazardous components are removed a-priori (such as screens and batteries) and the remaining electronic components are shredded. The concentration of NdFeB material is quite low and it is difficult to up-concentrate it in an economic manner following shredding, and therefore it is lost.

With the growing use of electronics and electrification of transport, one wonders how the industry will adjust to meet a large, forecasted demand (will be discussed further in Estimates for Global Recycling). In fact, The International Energy Agency (IEA) estimates that EV sales will reach 44 million by the year 2030, and it is safe to assume that each vehicle will contain at least one electric motor designed for traction. This supposition is done disregarding all the other electronics on board the vehicle that require REEs, suggesting an extensive future demand for these elements. Furthermore, [11] have proposed through their analysis of REEs that the normal primary supply of REEs will be unable to meet demand scenarios by 2050. We may suppose that with the implementation of reliable, economically and environmentally friendly methods of recycling, even a fraction of this demand could be met, alleviating the stress on primary sources. In fact, the same authors have suggested that secondary supply from recycling can meet almost 50% of the demand in the long term (around 2100).

Another aspect to consider as an incentive to recycling permanent magnets is the volatility of the REE market. A study made in 2010 by the United States Geological Survey (USGS) has estimated that global reserves of all rare earth oxides (REO) are estimated to be around 99 million tons, while the world production was 124000 t [12]. Here the term "reserve" has been defined for us: "the part of the reserve base which could be economically extracted or produced at the time of determination." Considering this, the reserve base is estimated to be at around 150 000 000 t of REO. This suggests that there is great potential to extract REEs from primary sources, however at a cost. Out of all the REO production, China produces 120000 t per year, a 97% share, while Brazil, India, and Malaysia account for 650, 2700, and 380 t per year respectively. In addition, 75-80% of Nd-FeB production occurs in China, while 17-25% occurs in Japan and 3-5% in Europe.

These statistics indicate a requirement for a decreased dependency on a single nation for the production of material and final product, and thus potentially decreasing the volatility in cost of REEs. An interesting aspect to consider is that the Chinese market drives the demand for many NdFeB applications, so EOL magnets as well as production scrap is most likely to arise in large quantities in China. With this in mind, proper collaborative strategies must be considered for the future to avoid cost volatility of the secondary material market.

ERECON has suggested that recycling EOL NdFeB magnet material arising in Europe could meet the demand of local magnet producers, however this may take time. Common findings among studies show that recycling will not be able to meet a large fraction of REE supply in the near future, however this fraction is increasing with a delay due to the time lag associated with product lifetimes and predicted growth of NdFeB applications.

2.3 Estimates of global recycling

With the most prevalent incentives having been discussed, estimates for the future concerning global recycling of the materials necessary for NdFeB magnets may be examined. Studies [13] indicate a forecast for higher demand of REE magnets and Dy for clean energy and transportation, where in general magnet production is projected to reach 99500 tons by 2035. Again, this is an extensive source of material that has the potential to be recycled, but one must look at the fraction that can feasibly be recovered. For this a study performed by Schulze and Buchert [14] may be referred to.

Firstly, the authours make several assumptions in order to model their estimates, in particular a direct recycling route was adopted for hard disk drives (HDD) and an indirect recycling route for every other product (recycling methods are discussed further in the following subsection). In addition, recycling potentials have been assumed to be derived from volumes of different EOL appliances containing magnets and that magnets are demanded and supplied in the same year. For each year considered, the global supply meets demand of rare earth metals (REM) through a combination of primary and secondary sources as well as secondary NdFeB material. Finally, no stockpiling of material has been assumed, where NdFeB material is recycled and made available as secondary material in the same year.

The paper makes a distinction for two scenarios: Low NdFeB demand and High NdFeB demand. The former considers only the fraction of REM demanded for use in magnets and that there is a slower progress of HREE content reduction. The latter considers a global application of REM (for magnets as well as other applications) and a faster progress in HREE reduction. It must be noted that the reduction of HREEs is an accepted goal in industry in order to minimize magnet production costs as discussed earlier, however it is uncertain at what rate this minimization will occur.

With the assumptions made in order to simplify the problem, the results show that the overall demand for NdFeB could increase by a factor of **three** for the

low demand scenario and a factor of **six** for the high demand considering 2015 levels as a base. This translates to around 80-112 kt in 2015 to 240 kt (low demand) and 633 kt (high demand) for the year 2030. Regarding the materials for the production of magnets, an estimate of around 7-11 kt of HREEs and 86-234 kt of LREEs will be required by the same year. Of these demands, 18-22% of global LREEs and 20-23% of HREEs used in NdFeB magnet production can be met from secondary sources, a combination of EOL magnets and industrial scrap.

With these promising numbers, one must take care to consider the number of assumptions that were taken into account in order to achieve them. They are indicative of trends that are likely to occur, however global recycling may be higher or lower than these estimates as government policies may sway producers to choose primary or secondary sources depending on what they entail. Objectively speaking, there is a great potential for recycling permanent magnets and given economically stable methods that entice OEMs coupled with political and environmental incentives, the predicted numbers may truly be met.

2.4 Recycling methods and potential application to the automotive industry

Knowing the great potential for recycling magnets, the possible methodologies for their recycling may be explored. However, one must firstly consider the difficulties associated with recycling. Generally, magnets can be removed using heat removal techniques, where the rotor is heated to decompose the adhesive. This comes with an issue: adhesives normally melt at 200°C, however they must be first demagnetized at around 300°C. Thus, the magnets can fly out uncontrollably from the rotor and damage themselves (as they are brittle) along with the heating stove. A temperature resistant fixation is needed to avoid this problem. Environmental concerns are also present, where decomposition techniques can lead to heavy smoke production, and when removing remaining bonding materials after heat treatment chemicals such as NaOH, boiling dimethylformamide and acetone are sprayed on the surface. In addition, these substances pose a health hazard to operators working on the extraction of the magnet material.

EOMs and recycling companies face certain economic and logistical obstacles considering magnet recycling as presented by [15]:

1. High plant investment and long disassembly process.
2. Requirement of additional processing techniques for the adhesives and Ni coatings typically on the magnets (as they corrode easily) where chemicals

used may be a health hazard.

3. NdFeB magnets are brittle and may easily be damaged.

4. Magnet shapes need additional machining to meet physical dimension specifications of new electric machines.

Therefore, some companies are stockpiling HDDs and other sources of material until there arises a viable economic method in recycling.

The two types of routes that exist currently are direct and indirect recycling. The former is concerned with reprocessing magnetic material into new magnets, while the latter relates to chemical decomposition of the magnets and the subsequent extraction of (individual) REEs. Direct recycling methods include hydrogen decrepitation (HD), complete magnet reuse, and a so-called "Lego" design, while indirect recycling routes include pyrometallurgical and hydrometallurgical methods. A study by [16] has shown that hydrogen decrepitation can be a promising solution for magnet extraction from HDDs, and it can be proven to be useful for motors without special design for disassembly. Therefore, this method will mainly be discussed with its application to the automotive industry, as well as other direct recycling routes.

2.4.1 Direct recycling routes

Complete magnet reuse seems to be a solution to certain issues highlighted earlier, where there may be complete reuse of magnets and rotor rings, eliminating the need for additional processing techniques. However, in light of novel motors, this poses a limitation: the designer has to work with the magnets in their primary dimensions. This leads us to the "Lego design" which has the concept of splitting a solid magnet pole into small standardized segments. These segments can then be used in different configurations within newly designed motors. Although it seems extremely practical, large amounts of adhesive are required and therefore a large cost associated to assembly is present. Furthermore, large repulsive forces between each segment occur when they are magnetized, and therefore need to be accounted for in the design of the motor.

Hydrogen decrepitation on the other and is a method concerned with the removal of NdFeB powder from magnets using hydrogen in a vessel. After this process, the hydrogenated material powder needs to be purified (removing all impurities), milled, and then sintered into new magnets following the commercial production route. With this method there is potential for enhancing the recovered magnet powder by adding a certain amount of virgin material (as typically properties

are lower after recovery). It is important to note that direct alloy recycling is not suitable for shredded material due to the high presence of contaminants. Typically, a re-sintered NdFeB material contains 2000-5000 ppm oxygen, while in comparison a primary cast NdFeB contains 300-400 ppm. This entire process is favorable to produce novel motors with recycled material due to its flexibility in design: the powder can be pressed into variable geometry meeting the physical dimensions of the motor. In addition, studies cited in [17] show that hydrogen decrepitation is more efficient as a process compared to indirect methods such as hydrometallurgical and pyrometallurgical methods where there is a higher consumption of energy and a higher consumption of chemicals respectively.

2.4.2 Automotive industry

The automotive industry has been highlighted as a major source of material, where greater than 7000 tons of NdFeB magnets in motors are used in EVs and HEVs. A single EV in 2012 contained around 4-5 kg of REE compared to less than a kilogram in a new petrol/diesel car [9]. Along with wind turbine generators, larger motors can be dismantled more easily, however this is not always the case. Smaller motors that contain typically 40 magnets which amount to around 250 g of NdFeB, may not be pre-dismantled prior to the car shredder and therefore are lost to ferrous and nonferrous scrap in a similar way to consumer electronics.

However, given the larger sizes of EV and HEV motors as well as their large content of recyclable magnets compared to other sources, they must be kept in mind. In fact, a study [9] has examined the extraction of material from an EM rotor, proving it to be relatively successful. Furthermore, automotive scrap has the potential to contain NdFeB material with increased Dy content (and therefore has a high value), meaning that reprocessing this scrap for new motors used in EVs and HEVs has a considerable advantage. The REE composition of the EOL products is closer to the desired ratio of REE in the production of new magnets, and thus design costs may be reduced for the parties involved. In addition, life cycle analysis studies presented in [9] show that re-sintered magnets using hydrogen processing have an energy usage that is 88% less with respect to that of primary production.

A disadvantage with automotive motors is that they come in a wide range of designs which use different materials and magnets positioning, and therefore it is difficult to have a universal method for the extraction of NdFeB material. This makes the extraction of the magnets a labor-costly endeavor. Although the higher Dy content is a positive from the point of view of the design and manufacture of new rotors, there has been some discussion on processing times using hydrogen. [9] show that with higher Dy content the hydrogen decrepitation process is slower

as compared to without the HREE, and the authours suggest a higher processing pressure is necessary for these types of magnets. This undoubtedly comes with a higher energy cost, however the good news is that over time manufacturers have been decreasing the amount of Dy content in new motors.

2.5 Comparison with primary source magnets

Knowing the application potential to the automotive industry, an analysis of motors fitted with recycled permanent magnets needs to be addressed. In particular, a study [8] has performed exactly that, using a brushless direct current motor that is used in printing, robotics and material handling, for their experimentation. The authours report the production of the recycled magnets (RM) through a technique similar to hydrogen decrepitation: the magnets are demagnetized, the anticorrosion layer removed through abrasion, the recycled magnets were milled, and finally a virgin magnet powder is added (comprising 3at.%) and the mixture is homogenized in a hydrogen-mixing reactor. The powder is then compacted and sintered into new magnets that are fitted into one of the motors, while the other motor is fitted with magnets produced from virgin magnet (VM) material.

The results following the characterization of the two motors report a flux linkage at open circuit that is 7% higher for the RM motor, as well as exhibiting an enhancement of coercivity of up to 80%. Furthermore, an improvement of motor efficiency is observed due to a reduction in eddy currents and therefore in the reversed magnetic fields generated during operation. In general, at higher temperatures, a motor demands more current to deliver a given torque. With increased current comes increased losses that further raise the temperature of the machine, until equilibrium is established. The RMs in this study are noted to have a lower Dy content, however the performance with respect to the VM motor is not impaired. In fact, there are no overall differences in the operating characteristics of the motors, the advantage is that the RM motor has a lower cost.

In addition to performance studies made recently, life cycle assessments (LCA) have also been performed to understand the impact recycled magnets have environmentally compared to virgin magnets. A study [17] looks at a LCA comparison between the production of 1 kg of virgin NdFeB magnets and 1 kg of recycled magnets suitable for high temperature applications (EVs and HEVs), considering a cradle-to-gate approach. This entails a process starting from the extraction to the factory gate. It considers HDDs as the target recycled EOL product, collected from data centers around the US that are assumed to be dismantled using an automated process to efficiently retrieve the NdFeB magnets. Along with assumptions

made on the transportation distances for the processing of the recycled materials, these suppositions affect the LCA where one does not get an exact quantitative measurement of each environmental impact. However, this can be seen as inherent to the LCA, where assumptions are made to simplify the scenarios. In addition, the process for recycling that is supposed is exactly the one reported by [8], and it is observed to have fewer steps as compared to that of virgin magnet production. It must be noted that the authours use ISO standards for the analysis: ISO 14040 and ISO 14044.

The results from the study show that the recovery of REEs during recycling is 90% or better and that the total virgin rare earth material used in the process is less than 5% (one may imagine reduced mining activity and energy). The recycling approach also exhibits about 31% to 55% of the environmental impact per category with respect to primary production, seen in Table 2.1. It is reported that for global warming, CO_2 from fossil fuels is the biggest source, while for acidification and respiratory effects are due to SO_2. Regarding the impacts for the recycling route, the majority of those that are significant are associated with virgin materials added to enhance the magnetic properties. Due to the small quantities involved, the recycling approach creates significantly less environmental impact compared to VM production. These are promising results, although they are based on many assumptions. Further studies will be necessary to determine with higher accuracy the effects that both production processes have on the environment, suggesting a close collaboration between industries and institutions involved.

Impact Category	Unit	Virgin	Recycled
Global Warming	kgCO_2 eq	27.602	12.453
Acidification	H^+ moles eq	20.524	11.320
Carcinogenics	benzen eq	0.069	0.035
Non carcinogenics	toluene eq	249.382	136.075
Respiratory effects	kgPM2.5 eq	0.124	0.059
Eutrophication	kgN eq	0.011	0.004
Ozone depletion	kgCFC-11 eq	1.25E-06	4.89E-07
Ecotoxicity	kg2.4-D eq	94.285	45.345
Smog	kgNO_x eq	0.109	0.034

Table 2.1: LCA results by category (after Jin et al., 2016)

2.6 Verdict

Recycling permanent magnets comes with many challenges currently, however given the vast potential outlined thus far, it is a venture that must be pursued. Incentives such as China's market dominance and the environmental benefits that comes with the recovery of NdFeB material lead one to conclude that there is a need for greater involvement from policy makers in order to promote this production route. It has been shown that RM motors have major benefits in terms of cost when compared to their VM counterparts. In addition, LCAs have indicated that the energy and pollutants emitted through the recycling route of magnet production are much lower when compared with the virgin magnets production, a finding that is incredibly relevant in this era where a great amount of focus is given to mitigating global temperature increases.

With the great potential in recycling present in the automotive and consumer electronics industries, OEMs have the opportunity to reduce costs in equipment production and therefore the two sectors seem as the most promising areas for NdFeB recovery to become prominent. With greater collaboration between OEMs and leading institutions worldwide, the 'urban mine' may soon become a viable source of material to alleviate the growing demand for permanent magnets.

Chapter 3

System Modelling and Control

The following chapter presents the system model along with all the relevant parameters used for the dynamic testing of the EM at vehicle level. The objective is to possess a robust representation of the real-world case, enough so as to produce reliable results that offer a strong suggestion of the efficiency of the RM machine compared to the VM machine when implemented on a hybrid powertrain. Certain control strategies are examined that lead to the introduction of the selected one for the application, in addition to the presentation of the vehicle model and the controller.

3.1 Control strategies

To obtain the peak performance of a HEV and reduce fuel consumption further with respect to conventional vehicles, energy management strategies are implemented. With the presence of an additional power source, being the battery, an efficient splitting of the power demand between said component and the ICE must be considered. This can be done in two ways: component level control or supervisory control. The former concerns itself with the control of each powertrain component through conventional feedback methods, while the latter considers the optimal energy flow within the vehicle. It is termed as the Energy Management System (EMS), and is responsible for the power split on board at each instant of the driving pattern to achieve the torque for the EM and the ICE. Furthermore, one main goal of such system is to maintain the state of charge (SOC) of the vehicle within a certain range of operation, meaning it must take care of not just energy distribution, but also the braking energy recovery.

The EMS may be classified into a certain number of categories that offer advantages and disadvantages. To arrive to the strategy for this application, it is necessary to briefly outline the various options available to automakers. However the main principle of these systems still stands, where the dynamic model of an HEV [18] in continuous and discrete time respectively is expressed through the following equations:

$$\dot{x} = f(x(k), u(t)), \quad 0 \leqslant t \leqslant T \tag{3.1}$$

$$x(k+1) = f(x(k), u(k)), \quad k = 1,2,...,N \tag{3.2}$$

The energy management problem may be described as:

$$\underset{x,u}{min} J, \quad s.t. \quad G(x) \leqslant 0 \tag{3.3}$$

where $x \in X$ is the state variable of the system, $u \in U$ is the control variable and $G(x)$ is the constraint condition. The control objective of the energy management problems is given by the cost function $J(x, u)$. The two most popular strategies are: rule-based and optimisation-based, their breakdown visible in Figure 3.1 from [18].

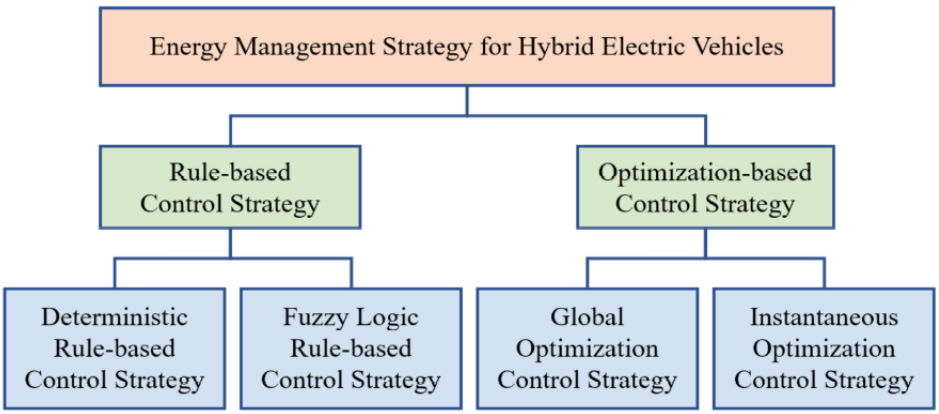

Figure 3.1: Control strategies for HEVs breakdown, after Xue et. al., 2020

3.1.1 Rule-based

Also called the logic threshold-based strategy, it uses a set of static parameters that have been obtained through experiments or engineering experience to define the optimal working area of the engine. The strategy determines the operating condition of the powertrain based on a set of predefined rules, meaning it is able to be implemented in real time operation in the vehicle. In addition, it is simple and

has good robustness, and thus is widely used in HEVs. However a notable downside to be outlined is that it is unable to adapt dynamically to changes in the driving conditions and therefore the HEV is unable to achieve maximum efficiency. Three modes exist: electric vehicle (EV), charge depleting (CD) and charge sustaining (CS).

Two main subsections of this type of strategy exist, namely **deterministic** and **fuzzy logic rule-based**. The former determines the working area and mode of the engine and the EM by setting threshold values for relevant vehicle parameters (SOC, power demand, vehicle speed), controlling the output of each power source based on predetermined control rules. The latter is based on fuzzy reasoning, and has the ability to control issues related to linear time invariant systems. With inputs of state variables such as SOC, the fuzzy reasoning determines the power distribution between the engine and the EM.

3.1.2 Optimisation-based

The main objective of the optimisation-based strategy is to solve an optimisation model based on an optimisation function. Currently the two main variants of this method are: instantaneous and global. Beginning with the **instantaneous** strategy, the working characteristics of the engine and the EM/battery pack are considered at each time step to minimise the total power loss of the vehicle and distribute the power or torque between the two power units. In particular, the strategy focuses on adjusting the output torque of the EM and engine to reduce the fuel consumption of the ICE and the equivalent fuel consumption of the EM. The general form of the instantaneous optimisation based strategy is as follows:

$$\begin{cases} u^{opt} = \underset{u}{argmin} J \\ J = f(u) + sg(u) \\ h(u) \leqslant 0 \end{cases} \tag{3.4}$$

where u is the control variable, J is the objective function, $f(u)$ is the fuel consumption of the engine, $g(u)$ is the power consumption of the EM, s is the equivalence factor, and $h(u)$ is the constraint in the optimisation process. The equivalence factor within such a strategy is quite sensitive to driving conditions, with a large amount of literature proposing various real-time adjustment methods. The expression above forms the basis for the Equivalent Consumption Minimisation Strategy (ECMS), a basis routed in the Pontryagin Minimum Principle (PMP).

The **global** optimisation-based strategy on the other hand is optimal in theory, however requires knowledge of the driving conditions in advance, which suggests

a huge computational necessity. Three different methods exist at present: multi-criteria-based mathematical modelling, Bellman direct programming (DP) based, and classical variation method based. The DP strategy is widely studied in literature, its core principle being to transform complex, multi-level optimisation issues into multi-level, single step optimisation problems. Because it requires the driving cycle input a-priori, it is not able to be used for online HEV control directly.

3.2 Model

The following section discusses the forward model of the P2 hybrid powertrain that is implemented on a LDV in Simulink®. This type of model offers the advantage of being more accurate in comparison to a backward model, however computationally heavier. This is due to the presence of the driver block, as opposed to the lack of it in the backward model where the speed of the vehicle is exactly that of the reference provideed by the driving cycle. The model is generalised into two subsystems: controller and plant. The former, as can be incurred by the name, has the purpose of controlling the latter, which represents all the physical phenomena of the system (the vehicle). The complexity of this model is extensive, and therefore only the main aspects that govern it are elaborated upon in depth. The various subsystems are visible in Figure 3.2 that depicts the general modelling structure for a P0, P1 and P2 configuration.

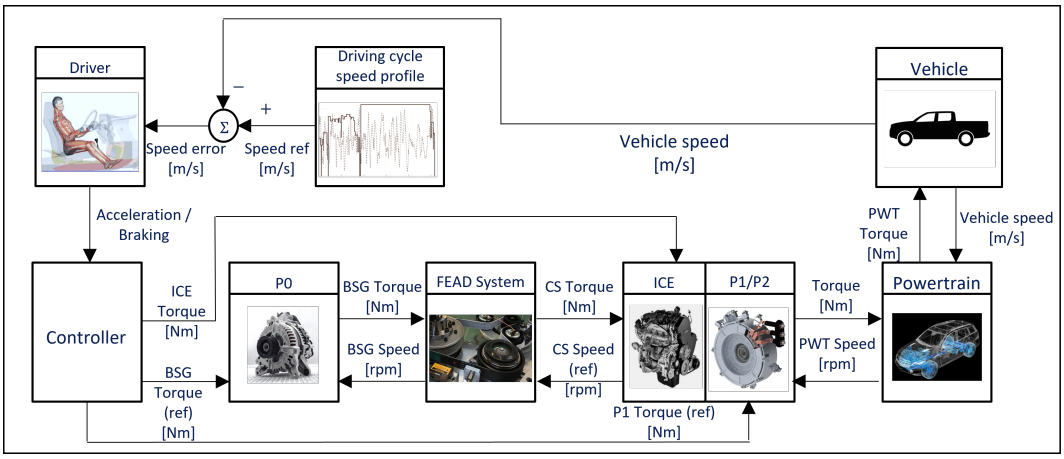

Figure 3.2: General modelling structure for P0, P1, P2 configurations

Generally speaking, the speed profile is represented by a standard homologation cycle, providing a velocity reference to the system. This value is summed at each time instant with the actual speed of the vehicle fed back from the plant to give an

error, which is subsequently fed to the model of the driver, (typically a PI controller) that generates a torque request. This signal is sent to the ECMS controller and in short: decides the level of usage of the P2 machine and the ICE. It produces as an output the throttle amount (ICE usage) and the P2 torque (EM usage) as the main parameters to control the plant. The vehicle subsystem that houses the powertrain model on the other hand generates (as one of the feedback parameters) the minimum and maximum available values of torque the machine may produce, depending on the lookup tables present. These tables are the torque-speed characteristics of the machine, particularly one is present for the motor mode and one for the generator mode. In addition, it provides a feedback of the angular speed of the ICE, the velocity of the vehicle and the state-of-charge (SOC) of the battery.

Figure 3.3 displays the controller and the plant of the model to be used, with all the feedback variables including the EM torque extremes being visible. It must be noted that this model incorporates a temperature feedback that has been added as an additional parameter to control the plant. This shall be discussed in full within the following sections.

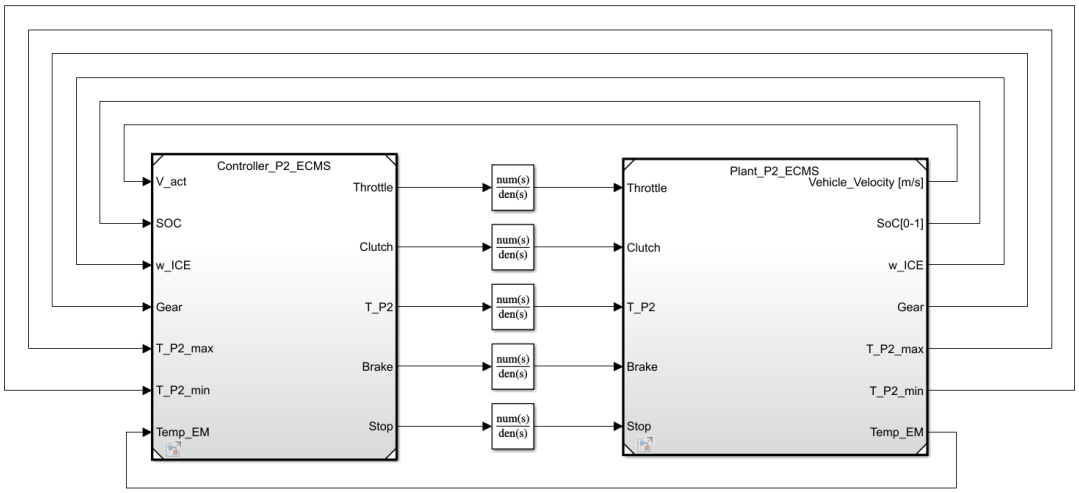

Figure 3.3: Simulink® model of controller and plant

3.2.1 Driving cycles

Various driving patters are present for the evaluation of fuel consumption and CO_2 emissions of vehicles, differing in aspects such as time duration, distance and average speed to name a few. Particularly, procedures exist for light and heavy duty vehicles, however only the cycles for the former shall be discussed. Some examples of dynamometer chassis tests include the Federal Test Procedure (FTP-75), the

Japan Cycle (JC-08), the New European Driving Cycle (NEDC) and the World Harmonised Light Vehicle Test Procedure (WLTP). The listed cycles are briefly described herein, with the intention to present the most relevant and updated type for testing of vehicles today.

Looking at the **FTP-75**, it consists of an urban route meaning a large amount of start-stops are present. It is made of three cycles: the first 505 seconds includes a cold start and an average speed of 41.2 km/h, while the second is 867 seconds long and the third is 505 seconds being identical to the first but with a hot start. Weighting factors of 0.43 and 0.57 are applied to the first and second phases respectively. The third phase starts after the engine is stopped for 10 minutes, Figure 3.4 displaying the various phases present.

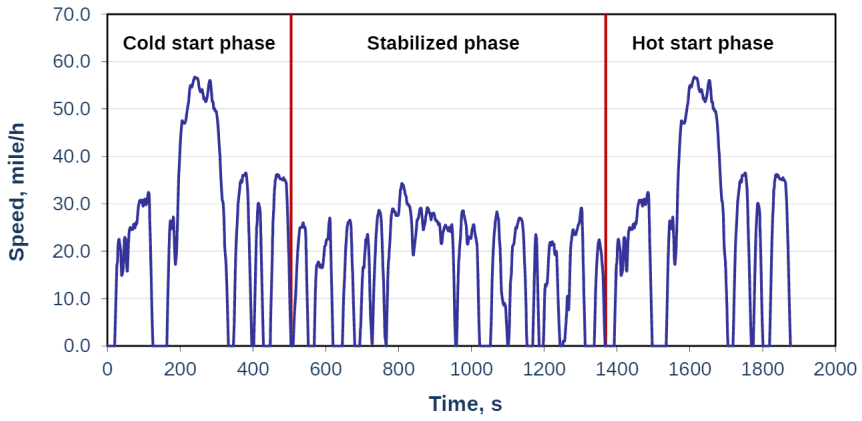

Figure 3.4: FTP-75 driving cycle

The **JC-08** has been developed by the Japanese emission regulation authority, representing congested city traffic that includes idling periods and frequent acceleration and deceleration. The test is broken down into a weighting of 25% cold start and 75% hot start. Figure 3.5 illustrates the driving schedule for this cycle.

Regarding the **NEDC**, this procedure has been developed by the European Union and is based on theoretical driving. It is composed of four repetitions of an urban cycle (ECE), devised to represent city driving conditions where the vehicle speed, engine load and exhaust gas temperature are low. The second phase is characterised by the Extra Urban Driving Cycle (EUDC) which accounts for more aggressive, high speed driving modes. Figure 3.6 displays the speed profile compositions.

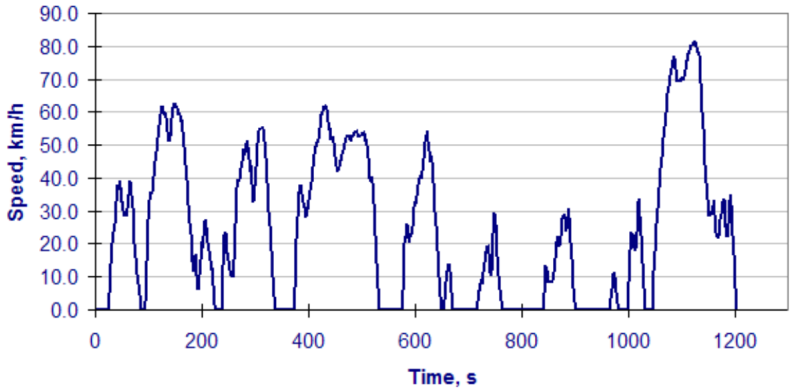

Figure 3.5: JC-08 velocity profile

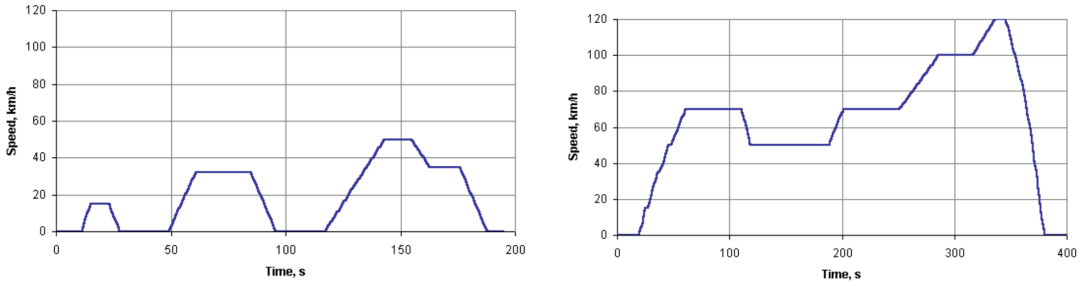

Figure 3.6: ECE (left) and EUDC (right) phases of the NDEC driving cycle

Finally, the **WLTP** cycle must be discussed, which is more strictly a set of cycles and procedures for different test cases (vehicle categories). It replaces the NEDC based procedure for LDV approval testing as it is based on real driving data. For the purpose of the application in this work, the WLTP3 procedure will be discussed. The cycle is broken down into four phases: Low, Medium, High and Extra High as can be seen in Figure 3.7. In these various phases, the representation of urban, rural and highway driving are present. Given the requisites of the EU for emission data collection based on tests outlined in Chapter 1, the WLTP3 is the drive cycle selected for the application at hand, as it is the most consolidated thus far.

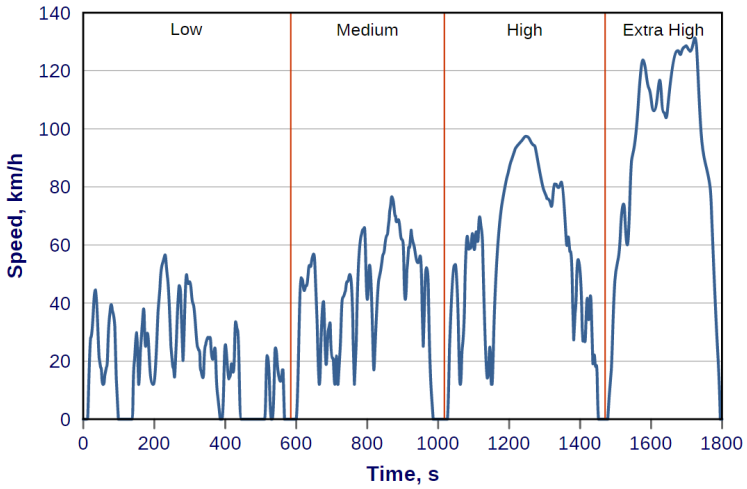

Figure 3.7: WLTP driving cycle

Parameter	FTP-75	JC-08	NEDC	WLTP3
Duration [s]	1877	1204	1180	1800
Distance [km]	17.77	8.171	10.931	23.266
Average speed [km/h]	34.12	34.8	33.35	51.78
Maximimum speed [km/h]	91.25	81.6	120	131.2

Table 3.1: Summary of main features of each driving cycle

3.2.2 Plant

Regarding the vehicle model, it may be broken down into several subsystems that generate specific feedback variables so that it is controlled in a proper manner. On the basis of theoretical reasoning, the required power of the vehicle is given as:

$$P_v = P_{grade} + P_{roll} + P_{drag} + P_{inertia} \tag{3.5}$$

where P_{grade} is the contribution due to grade resistance, P_{roll} takes into account the rolling resistance, P_{drag} is the power required to overcome aerodynamic drag and $P_{inertia}$ is the inertia resistance. These terms may be expressed in the following manner respectively:

$$P_{grade} = m_v \cdot g \cdot v_v \cdot \sin(\alpha_r) \tag{3.6}$$

$$P_{roll} = m_v \cdot g \cdot v_v \cdot r_v \cdot \cos(\alpha_r) \tag{3.7}$$

$$P_{drag} = (\frac{1}{2} \cdot \rho_{air} \cdot c_x \cdot A_v \cdot v_v^2) \cdot v_v \tag{3.8}$$

$$P_{inertia} = \left(m_v + \frac{I_{wh}}{R_{wh}}\right) \cdot v_v \cdot \dot{v}_v \tag{3.9}$$

where m_v is the mass of the vehicle, g is the gravitational acceleration and v_v is the vehicle velocity. The slope given by the driving cycle is represented by α_r, while r_v is the vehicle rolling friction coefficient, rho_{air} is the density of air and c_x is the vehicle drag coefficient. A_v is the frontal area of the vehicle and $\dot{v}_v$ is the vehicle acceleration. This power request (or torque request) must be satisfied by the ICE and the EM found on the powertrain. More practically, certain parameters of the vehicle indicated in the formulations are found in the longitudinal dynamics block of the model that is responsible for the computation of the actual speed that is fed back to the controller. Table 3.2 gives an overview of some of the main parameters that characterise the plant and that are initialised in a supporting MATLAB® code.

Parameter	Value
Mass [kg]	3100
Battery capacity [Ah]	17
Wheelbase [m]	3.3
Frontal area [m^2]	4.58
Wheel radius [m]	0.35
Friction coefficient	0.015
Drag coefficient	0.316
Gear number	8
Final gear ratio	3.615

Table 3.2: Vehicle parameters

For the correct control of the plant, various parameters are required to be used as inputs to the controller. Two of those parameters are the minimum and maximum torque that the machine may produce at a given time instant. These values are considered as one of the constraints of the control along with the maximum and minimum values of the SOC. The torque values returned to the controller depend on the use of look-up tables generated a-priori by providing as an input the instantaneous speed and temperature of the machine. These tables are built using a numerical approach for the static characterisation of the EM to produce torque-speed curves for each magnet temperature and are discussed further in Chapter 4. They are present within the powertrain block of the plant model. Figure 3.8 indicates the subsystem for the evaluation of the maximum and minimum torque values, as well as the power of the EM to compute the SOC.

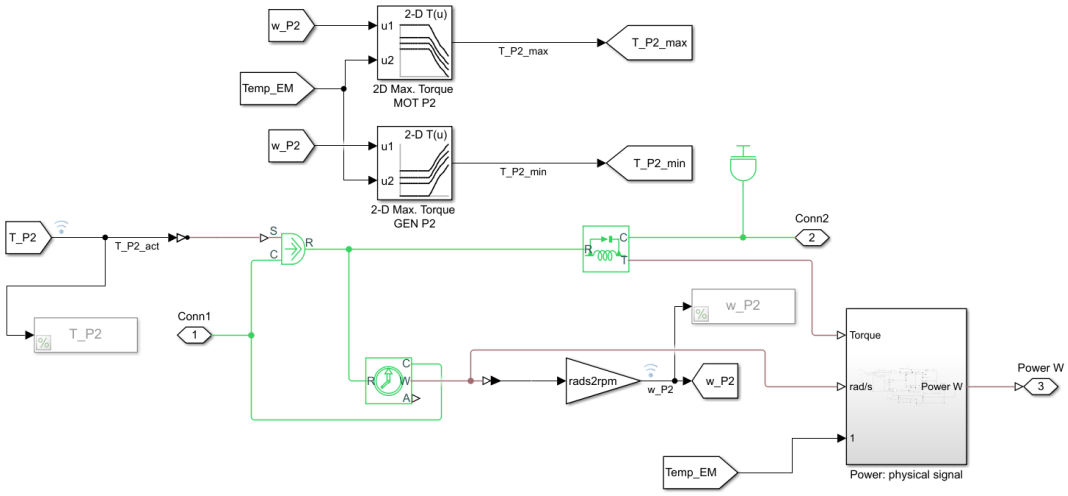

Figure 3.8: Minimum and maximum torque value computation subsystem

The **temperature** is computed in a unique way that involves the power losses of the machine, through a transfer function reported in the following expression:

$$\frac{\Delta Temp_{EM}}{P_{loss}} = \frac{k_{th}}{1+\tau s} \tag{3.10}$$

where $\Delta Temp_{EM}$, k_{th}, τ, and P_{loss} are the incremental temperature change, thermal coefficient, thermal time constant and power loss of the machine respectively. It is important to note that the output is only a temperature rise or fall, and therefore needs to be added to an environmental temperature to obtain the absolute value. Furthermore, the power losses also need to be evaluated, with the values in motoring and generating mode at each time instant computed through:

$$\begin{cases} P_{loss,M}(t) = \frac{T_{EM}(t)\cdot\omega(t)}{\eta_{EM}} \\ P_{loss,G}(t) = T_{EM}(t)\cdot\omega(t)\cdot\eta_{EM} \end{cases} \tag{3.11}$$

with $T_{EM}(t)$, η_{EM}, $\omega(t)$ being the torque, efficiency and angular speed of the machine. The two types of power losses are considered at every time instant (depending on whether the machine is in motoring or generating mode) to be fed into the transfer function to output the temperature increment. This value in turn is summed with an approximated engine bay temperature to obtain the final temperature of the EM.

The values of efficiency for motoring and generating modes of the EM are given as an output with the use of three dimensional look-up tables prepared prior, that are then referenced in the model. The three axes of these tables are the angular speed,

torque and temperature of the machine, suggesting a natural requirement of three inputs that are used to interpolate the data linearly to select the corresponding efficiency value.

Furthermore, the thermal model includes the representation of cooling of the machine. This is done through the use of the following expression:

$$P_{extracted} = \dot{m_{coolant}} c_p (Temp_{EM} - Temp_{coolant}) \tag{3.12}$$

where $\dot{m_{coolant}}$, c_p, and $Temp_{coolant}$ are the mass flow rate, specific heat capacity and temperature of the coolant respectively. $Temp_{EM}$ indicates the temperature of the EM. The mass flow rate is kept at a constant value, however the cooling is only initiated when the temperature of the machine exceeds a threshold. This is done to limit the additional load on the battery and prevent a continuous power request. The extracted power is subtracted from the power loss to obtain a lower temperature increment when active and thus representing cooling of the machine. In addition, the coolant used is a mixture of water and glycol and its temperature value is set at 70°C, meaning that the power extracted is only dependent on the temperature of the EM. The entire subsystem to calculate the instantaneous efficiency values along with the logic to compute the temperature is visible in Figure 3.9. The relevant parameters for the thermal model are presented in Table 3.3

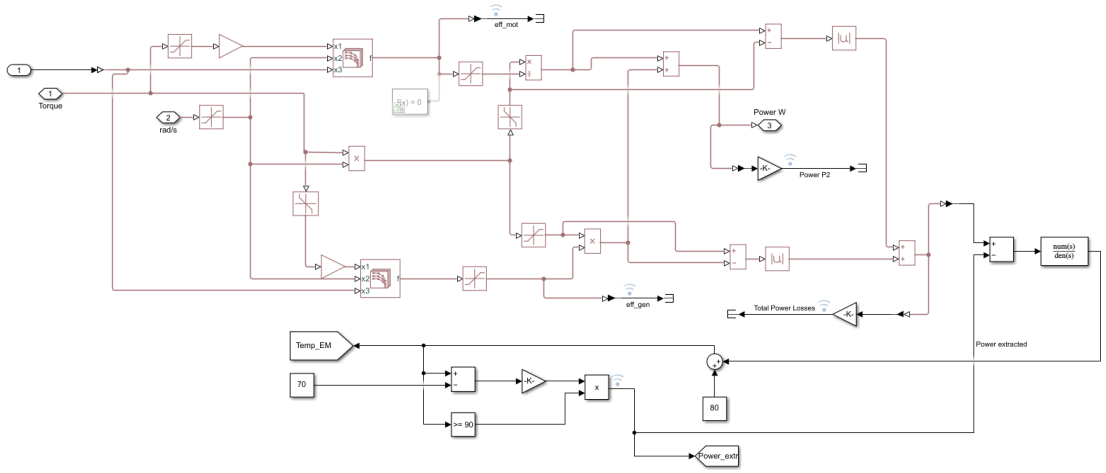

Figure 3.9: 3D look up tables and temperature computation subsystem

Finally, the battery is modelled as an ideal voltage source which varies with the SOC through the following relation [19]:

$$V = V_o \cdot \left(\frac{SOC}{1 - \beta(1 - SOC)}\right) \tag{3.13}$$

Parameter	Value
EM thermal coefficient [K/W]	0.1
EM thermal time constant [s]	386
Coolant mass flow rate [kg/s]	0.006
Coolant specific heat capacity [J/kgK]	3657
Coolant temperature [°C]	70
Threshold temperature [°C]	90

Table 3.3: Thermal model parameters

where V_o is the open circuit voltage at full battery capacity and β is a characteristic parameter. The battery block takes as an input the power request from the EM and the cooling system and generates the corresponding SOC as an output for each time instant.

3.2.3 ECMS controller

With a brief introduction to control strategies having been presented, the strategy for the application must be examined. Recalling the general formulation of the optimisation-based strategy in Equation 3.6, the total objective function of the vehicle to be minimised may be expressed as:

$$\begin{cases} \sum_0^t J_{ECMS} \\ J_{ECMS} = \dot{m}_{fc} + s \cdot \dot{m}_{EM} \end{cases} \tag{3.14}$$

where $\dot{m}_{fc}$ is obtained from the interpolation of the engine map (Brake Specific Fuel Consumption (BSFC)) with the requested torque and speed of the ICE fed into the controller. This map reports the fuel consumption as a function of the angular speed and torque. The formulation for the ICE mass flow rate is:

$$\dot{m}_{fc} = \dot{m}_{fc}(P_{ICE}, \omega_{ICE}) \tag{3.15}$$

while the equivalent mass flow rate of the electric machine may be written as follows:

$$\dot{m}_{EM} = \frac{P_{EM}}{\eta_{EM} \cdot Q_f} \tag{3.16}$$

where P_{EM} is the power of the electric machine and Q_f is the lower heating value of the fuel. The instantaneous value of the EM power is computed using the requested torque and the speed of the machine fed into the controller:

$$P_{EM}(t) = T_{req} \cdot \omega(t) \cdot u(t) \tag{3.17}$$

It is important to note that the formulation in Equation 3.16 is with regards to the traction operation of the machine, with the control variable $u(t)$ seen in Equation 3.17 expressed as:

$$\begin{cases} u(t) = \frac{T_{EM}(t)}{T_{req}(t)} \\ T_{ICE} = (1 - u(t)) \cdot T_{req} \\ T_{EM} = u(t) \cdot T_{req} \end{cases} \tag{3.18}$$

The instantaneous efficiency is obtained with the torque-speed and efficiency map which is interpolated linearly using the requested torque and speed as seen through:

$$\eta_{EM} = \eta_{EM}(T_{req} \cdot u(t), \omega_{EM}) \tag{3.19}$$

This value is subsequently used in Equation 3.16 to obtain the EM mass flow rate. At each time instant a vector of control variables is generated that is used to obtain the ICE and EM flow rates from their respective maps. A vector of equivalent mass flow rates is computed from which the minimum value is extracted, corresponding to the control variable that facilitates this. The chosen value of $u(t)$ is then used in Equation 3.18 to compute the ICE and EM torque.

During the minimisation of the fuel consumption, certain variables must be monitored. Arguably the most important parameter considering HEV control is the SOC of the battery where certain considerations on its value must be accounted for. Particularly, the initial and final charges must be as close to each other as possible, ideally being the same. This is due to the fact that the battery is not externally rechargeable and should guarantee the power necessary to facilitate a pure electric start of the vehicle if necessary. If the SOC is below the imposed threshold at the end of the driving cycle, the result is the fuel consumption is lower than expected (thus misleading) and more fuel is required to bring the SOC back to the threshold value. Furthermore, ideally the SOC must fluctuate between maximum and minimum bounds to guarantee a proper value of charge should the engine be switched off at any point, and to prolong the life of the battery. These values these parameters are reported in Table 3.4.

Considering this, the penalty factor should be expressed in terms of the variation of the SOC, given by the following expression:

$$s(t) = s_{0,dis} + k_{p,batt}(SOC_{ref} - SOC(t)) \tag{3.20}$$

where $s_{0,dis}$ is the discharge constant, $k_{p,batt}$ is the tuneable parameter, SOC_{ref} is the reference state of charge, and $SOC(t)$ is the instantaneous state of charge fed back from the plant. One aspect to note is that this linear equation requires the proper combination of two parameters ($s_{0,dis}$ and $k_{p,batt}$) for the obtention of a

suitable penalty value. This entails a trial and error process, which may be lengthy if the starting values are chosen too far away from those most ideal to obtain a final SOC equal to that of the initial. However the shooting method may be used to give a starting point for one of the parameters, and the following parameter can be made as a function of the first in a tuning process. Another method to evaluate the parameters is through a genetic algorithm that is integrated with the model, where initial values may be implemented from which the optimal ones will be generated. An example of this type of implementation may be seen in Figure 3.10 where the authors in [20] solve for a family of coefficients that defined their own penalty function with respect to the SOC.

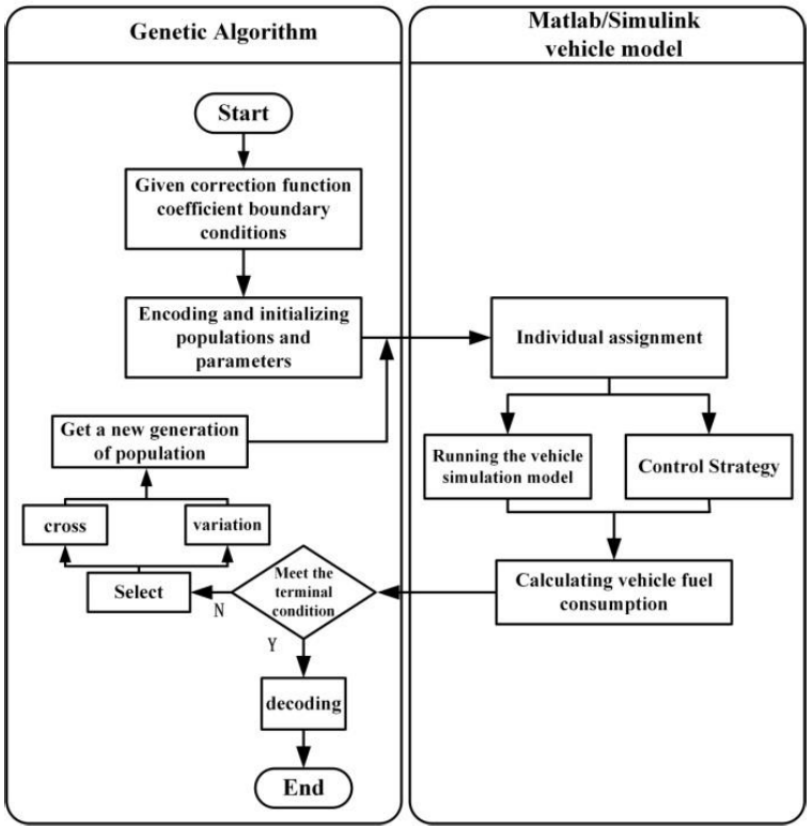

Figure 3.10: GA incorporation with ECMS, after Liu et al., 2019

For this work the shooting method is employed to determine the constant parameter $s_{0,dis}$ through the following formulation as reported in [19]:

$$\begin{cases} s_{0,dis}(t) = \frac{1}{2} \cdot (S_d(t-1) + S_u(t-1)) \\ S_d(t) = S_{dis}(t-1); & \text{if } SOC_{final} - SOC_{ref} < 0 \\ S_u(t) = S_u(t-1); & \text{if } SOC_{final} - SOC_{ref} < 0 \\ S_d(t) = S_d(t-1); & \text{if } SOC_{final} - SOC_{ref} > 0 \\ S_u(t) = S_{dis}(t-1); & \text{if } SOC_{final} - SOC_{ref} > 0 \end{cases} \tag{3.21}$$

where S_d and S_u are arbitrary variables that are initialised and updated at every iteration to be then used in the bisection formulation. Each iteration consists of assigning the constant to the model and running it in its entirety. The optimisation ends when the difference between the final SOC and the reference SOC is below 0.1%. Once the value is obtained, the tuneable parameter is found through:

$$k_{p,batt} = 0.00875 \cdot s_{0,dis} \tag{3.22}$$

The initial parameters as well as the final obtained parameters are reported in Table 3.4.

Parameter	Value
$s_{0,dis}$	2.8
$k_{p,batt}$	0.0245
S_d	0
S_u	4
$S_{initial}$	2
SOC_{ref} [%]	60
SOC_{min} [%]	20
SOC_{max} [%]	90

Table 3.4: Shooting method parameters for baseline ECMS

Finally, the minimum and maximum torque values available at each time instant that are fed back from the plant must be respected, a constraint the ECMS must abide by. In addition, the reasoning set forth thus far has been for the case of the machine operating in motoring mode. Regarding the recuperation mode, that is when the requested torque is below zero, the following relation must be followed:

$$T_{EM} = max(T_{req}, T_{EM,min}) \tag{3.23}$$

where $T_{EM,min}$ is the available generator torque, being the minimum torque value discussed earlier. The flow logic presented to this point is seen in Figure 3.11. The

full set of constraints are summarised from [19] as follows:

$$\begin{cases} T_{req}(t) = T_{ICE}(t) + T_{EM}(t) \\ 0 \leqslant T_{ICE}(t) \leqslant T_{ICE}(\omega_{EM}) \\ T_{EM,min}(\omega_{EM}) \leqslant T_{EM}(t) \leqslant T_{EM,max}(\omega_{EM}) \\ SOC_{min} \leqslant SOC(t) \leqslant SOC_{max} \end{cases} \tag{3.24}$$

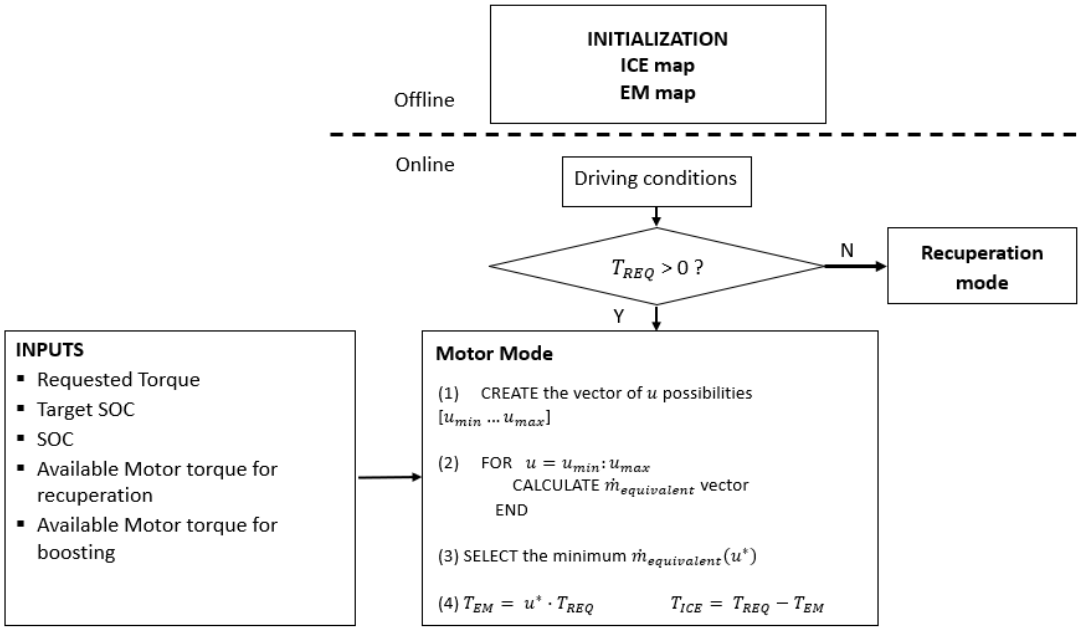

Figure 3.11: ECMS logic

3.2.4 Developed ECMS controller

The formulation in Equation 3.20 considers the variation of the SOC alone, however during the operation of the vehicle, variation of the EM temperature is bound to occur due to its periodic use. This leads to a degradation of the machine's performance for reasons discussed earlier. To take this into account, one can modify the expression of the penalty factor to include the variation of the EM temperature with respect to a reference value:

$$s(t) = s_{0,dis} + k_{p,batt}(SOC_{ref} - SOC(t)) - k_{p,temp}(Temp_{ref} - Temp(t)) \tag{3.25}$$

where $Temp_{ref}$, $Temp(t)$ and $k_{p,temp}$ are the reference temperature, instantaneous temperature and the temperature tuning factor respectively. The formulation gives

an indication on how the penalty factor varies: with the temperature increasing above the reference value, the factor decreases and vice versa. Likewise for the SOC, as the instantaneous SOC decreases below that of the reference, the factor increases and thus penalising the use of the machine to a greater extent.

For the correct operation of the system in terms of SOC and temperature variation, the additional tunable parameter must be adjusted with respect to the ones already present. The shooting method with the same initial parameters as for the baseline ECMS is exploited again to first find the constant $s_{0,dis}$ and then the two tuneable parameters are adjusted and found through:

$$\begin{cases} k_{p,batt} = 0.00725 \cdot s_{0,dis} \\ k_{p,temp} = 0.0075 \cdot s_{0,dis} \end{cases} \tag{3.26}$$

The same logic is used for this ECMS as for the baseline (Figure 3.11) where the only additional input parameter is the temperature of the machine. This value is used at each time instant by the three dimensional map present in the controller that represents the EM to obtain the efficiency that is subsequently used to compute the mass flow rate of the EM as seen in Equation 3.16. Table 3.5 contains the final parameters of Equation 3.25.

Parameter	Value
$s_{0,dis}$	2.806
$k_{p,batt}$	0.020
$k_{p,temp}$	0.021
$Temp_{ref}$ [°C]	90

Table 3.5: Developed ECMS parameters

Chapter 4

Testing Methodology

To define a thorough testing methodology of the two Physis PMSMs (one with VMs and the other with RMs), one must address the objectives. In particular they are twofold: obtain the EM static and dynamic performance. The former has the aim to generate the torque-speed characteristic and the efficiency map. The latter concerns itself with obtaining the fuel consumption of the vehicle with the two machines implemented on a P2 hybrid powertrain. However, the robustness of the testing may be augmented with the inclusion of a numerical aspect including models such as the one discussed in Chapter 3 that can be tuned with respect to the results obtained from the experimental work. This would solidify a useful tool that can be used in the future of testing of such machines. Figure 4.1 exhibits the testing hierarchy to be adopted.

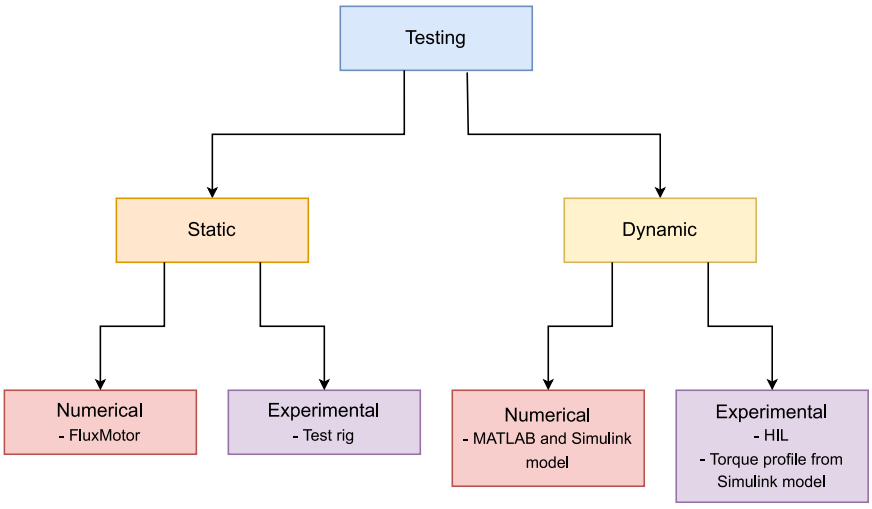

Figure 4.1: Testing structure

The experimental work is to be executed at the CARS test facility (seen in Figure 4.2), located in the main campus of the Politecnico di Torino. The rig is fully outfitted by AVL, an entity that concerns itself with the development and manufacture of testing solutions for automotive systems. The rig can be used for the static evaluation of EMs and has the potential to facilitate hardware-in-the-loop (HIL) set-ups through the integrated equipment present (will not be discussed here) to examine the dynamic performance of the machines. In addition a torque profile coming from a Simulink® model may be used and shall be discussed briefly in this chapter.

Figure 4.2: CARS Center test facility

4.1 Static characterisation

4.1.1 Numerical

This evaluation route is based on the physics of the machine, and uses at its core a finite element method (FEM) software called Altair FluxMotor®. For this path, there is a need for the 2D model of the machine to be built, to which the properties of the magnets used (and more generally the other materials) may be assigned. The concepts described in Chapter 1 for PMSM operation form the basis of the analytical simulation, such that the torque-speed characteristic and efficiency map may be generated.

To develop these results, the magnet data including the relative magnetic permeability and coercivity are required. As seen in the operating principles of PMSMs,

the magnet type affects the performance of the machine as the permanent flux linkage is directly dependant on remanent flux density (B_r). If this value decreases, the magnetic flux generated is lowered and subsequently the flux linkage as well (Equation 1.3). Furthermore, this directly affects the peak torque the machine may produce, where Equation 1.12 indicates a direct relationship between the torque and the permanent flux linkage.

The reasoning suggests that a machine with recycled permanent magnets would exhibit lower peak torque values as a minimum, with a forecasted decrease in efficiency. This would be due to the impurities that are present from the recycling process (seen in Chapter 2). Furthermore, the degradation of a magnet's properties also occurs with its increase in temperature, and therefore a machine's performance would decrease in this regard as well. In order to display this effect, the data of a magnet characterisation at various temperatures performed by Mondragon University (project partners) has been exploited.

The data is provided within an excel sheet containing the raw results of the characterisations. The test obtains the flux density (B_r) with respect to a variation of the coercive magnetic field (H), where a linear correlation between the two is extracted. This value is the relative magnetic permeability, and is provided in a summary table along with the remanent flux density and the coercivity. The main parameters are summarised in Table 4.1.

Parameter	25°C	80°C	100°C	120°C
Relative magnetic permeability (μ)	1.01	1.03	1.06	1.11
Coercivity (H) [kA/m]	1026.4	740.92	601.56	473.67

Table 4.1: Summary of the magnet parameters used to obtain torque speed maps

Regarding the behaviour of these parameters with respect to the magnet temperature, once graphed there are correlations for each that may be deduced. In particular, the coercivity is observed to have a negative linear behaviour with temperature increase as seen in Figure 4.3. By exploiting the expression:

$$B_r = \mu \cdot \mu_0 \cdot H_c \tag{4.1}$$

one is able to obtain the remanent flux density with respect to temperature, with μ_0 being the relative permeability of air. As anticipated, the relationship is negatively linear with increasing temperature, implying a degradation in machine performance. With this data fit, one is able to determine the remanent flux density for various

magnet temperatures and predict how the machine will behave (as a preliminary step). This may easily be extended to magnets with recycled material, where all that is required are the parameters discussed to be processed and plotted.

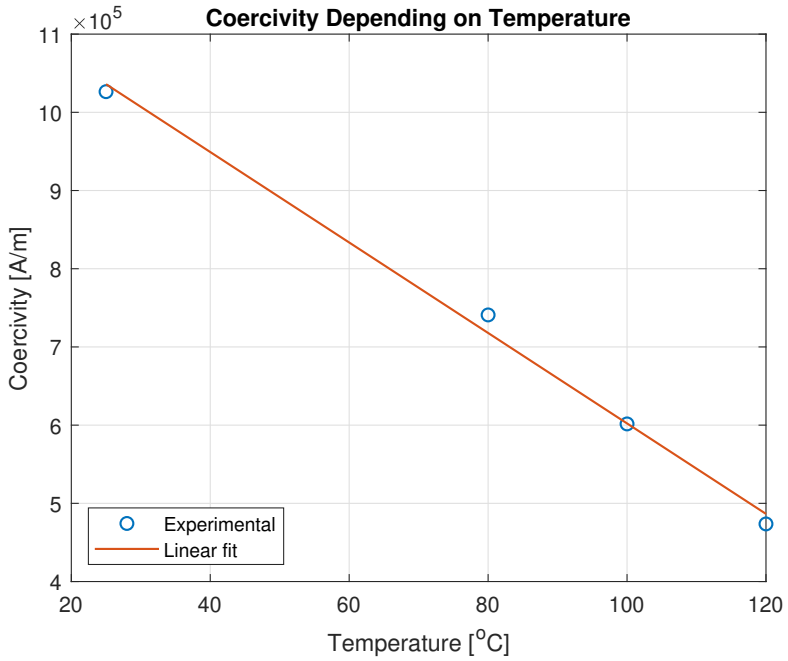

Figure 4.3: Variation of coercivity with temperature

Having discussed the effect of temperature on magnet properties, the resultant outcome regarding machine performance should be addressed. The case study here is a high voltage PMSM from a Toyota Prius 2010 and with the use of the dedicated FEM software, the characteristics of the machine at varying temperatures are obtained. Looking at Figures 4.5, 4.6, 4.7, 4.8, a clear degradation is evident. The peak torque curve decreases with subsequent increases in temperature, moving from around 130 Nm at 25°C to about 100 Nm at 120°C. Furthermore, a narrowing of the high efficiency region and a shifting of the lower efficiency regions to the right may be seen as the magnet temperature increases.

The effect of magnet temperature is notable, suggesting thermal management of EMs during operation is necessary. This is a feature already present in commercial solutions in the form of cooling jackets for example (typically water-glycol as the circulating coolant).

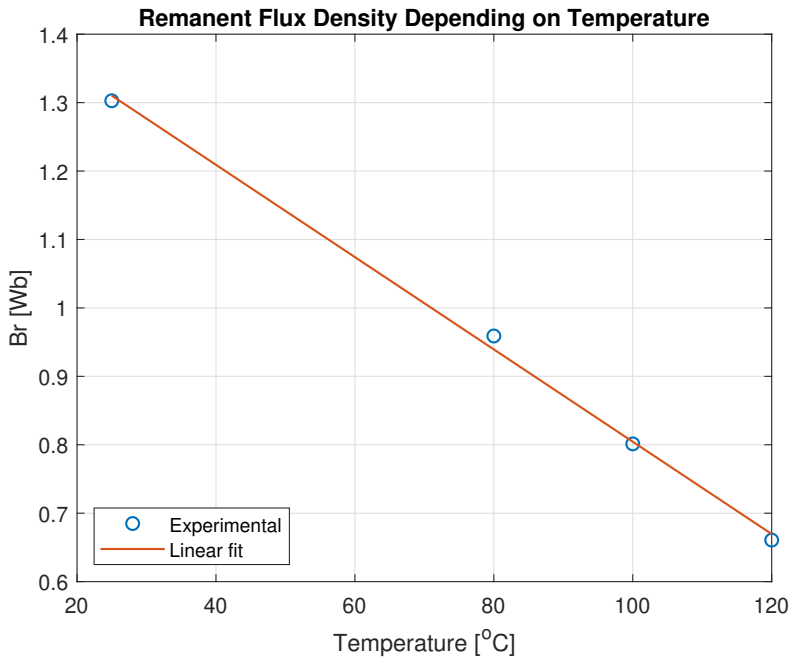

Figure 4.4: Variation of remanent flux density with temperature

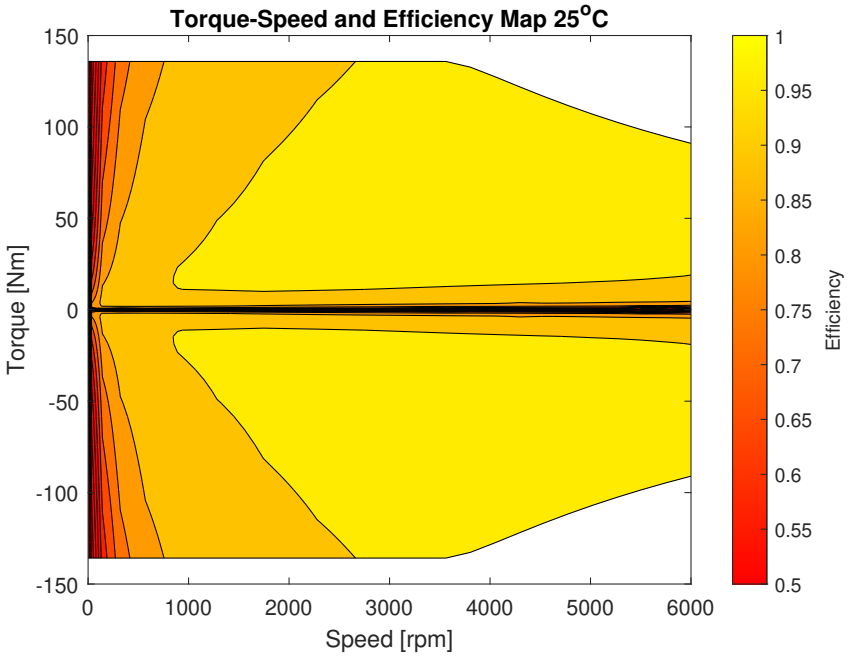

Figure 4.5: Prius machine characterised with magnet data at 25°C

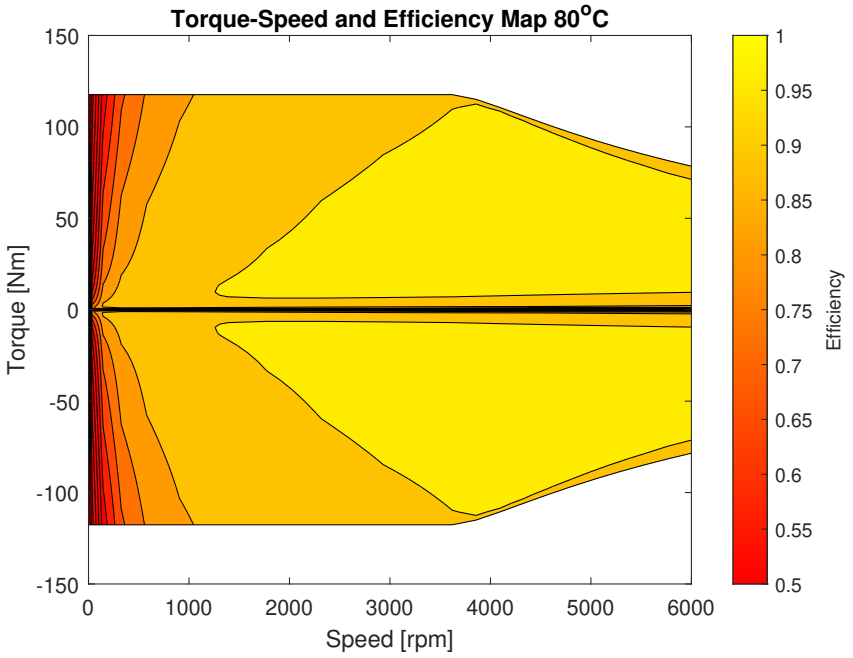

Figure 4.6: Prius machine characterised with magnet data at 80°C

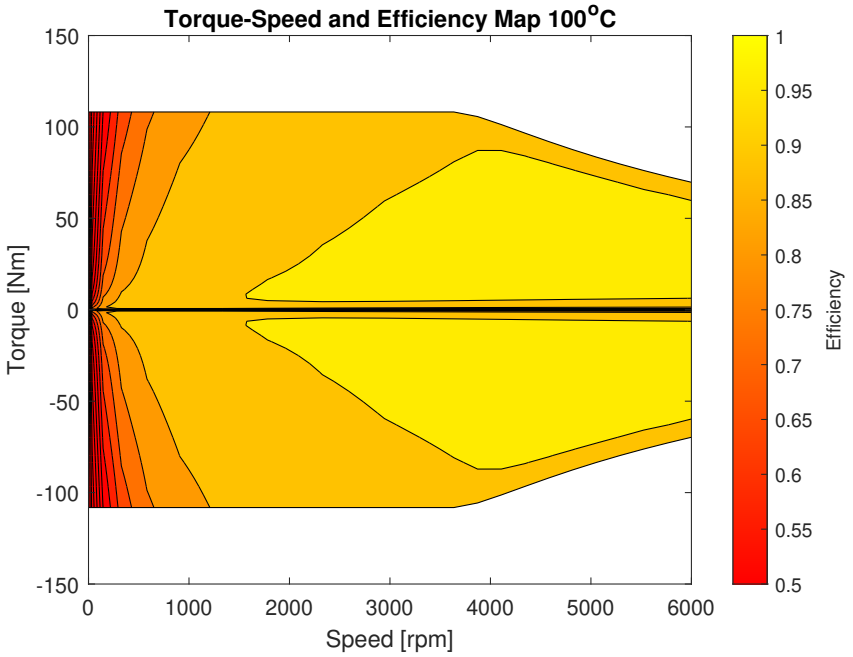

Figure 4.7: Prius machine characterised with magnet data at 100°C

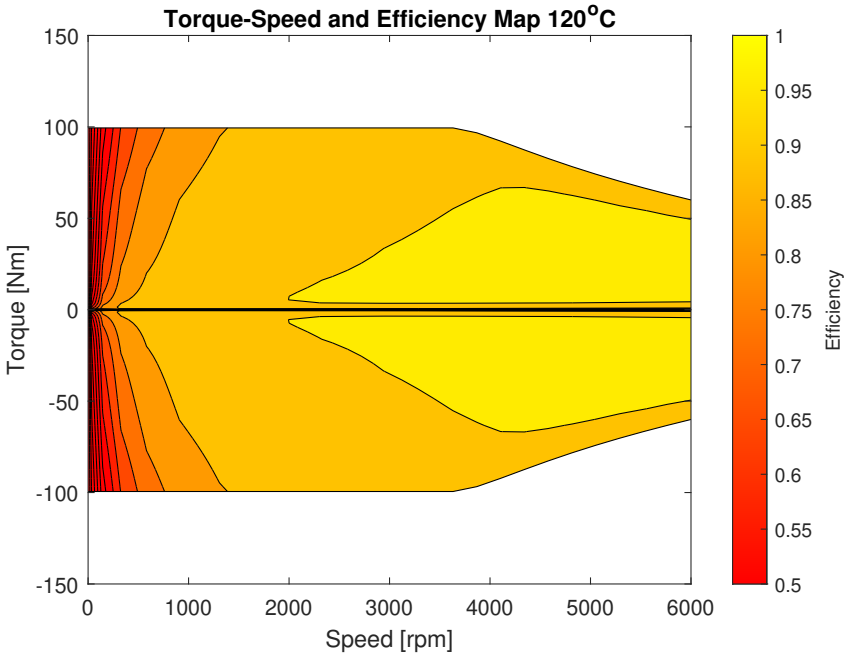

Figure 4.8: Prius machine characterised with magnet data at 120°C

4.1.2 Experimental

The use of a numerical model alone for the static characterisation of the EM is not enough in modern development of engineering solutions, giving rise to the need for experimental work. Numerical data obtained from the analysis of VM and RM EMs must be then confronted with experimental data obtained from physical tests of the two machines, such that the models may be verified. The layout for this type of testing includes certain equipment that must be addressed. Firstly, if the ICE is not available for testing purposes, the prime mover present in the test rig is used to emulate the engine. The said equipment displays appreciable features for this purpose, with the capability of delivering 800 Nm of torque from 0 to 5440 rpm. In addition, the machine (also a PMSM) is able to simulate various gear shifting methods such as automatic, continuous variable transmission (CVT) or manual. The EM is connected to this device by means of a mechanical coupling, a casing and a flange, components that are designed in the following section of this chapter. Furthermore, the EM is connected to a dedicated inverter that is in turn connected to a battery emulator present in the test cell.

The acquisition software used is AVL's in-house developed system named Indicom for e-power applications. The acquisition during the experimentation consists of:

1. Direct voltage and current at inverter inputs.

2. Phase width modulated (PWM) AC voltage signals (line-to-line) and phase currents that are recorded at inverter outputs. The sampling rates of the line-to-line voltages are 1 or 2 MHz, while the phase currents are 500 or 1 MHz.

3. One DC voltage (with inverter operation).

To obtain the required data, one must provide the correct inputs first, the most important of which are the pole pair number of the machine, the source (current, voltage or current/voltage) to compute the period detection, and the minimum current and voltage. The user is then prompted to select the set of outputs, which may be frequency, speed, torque-speed curve and efficiency to name a few. The testing set-up is outlined in Figure 4.9, while Figure 4.10 details the input and output selection windows of the software.

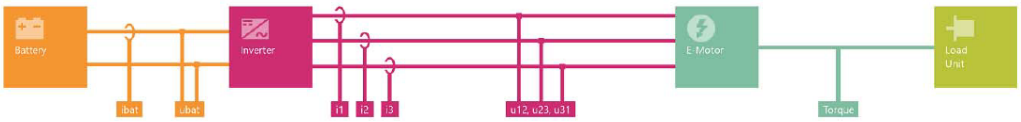

Figure 4.9: Testing layout

Figure 4.10: Input and output window of Indicom

4.1.3 Mechanical interface design

The mechanical connection between the EM and the prime mover needs to be defined. In particular, the output rotor of the EM needs to be coupled with the rotor of the prime mover by means of a commercially available flexible coupling. This connection is axial, and therefore the natural coupling of choice is of the bellow type. The selection of the component takes into account the maximum torque that

needs to be transmitted from one shaft to the other. Given this value is 330 Nm for this application, a WK4 300 bellow coupling was selected from the catalogue of STS Coupling, seen in Figure 4.11. As its name suggests, it is capable of transferring 300 Nm of torque, meaning the full operating envelope of the machine is unable to be evaluated. Thus the WK4 500 was also ordered to allow for the ability to reach the peak torque value. The two couplings were ordered in the 'blind' configuration, meaning the bores are simply pilot holes that have been machined within the Dayco workshop with the diameters of the EM rotor and flange considered.

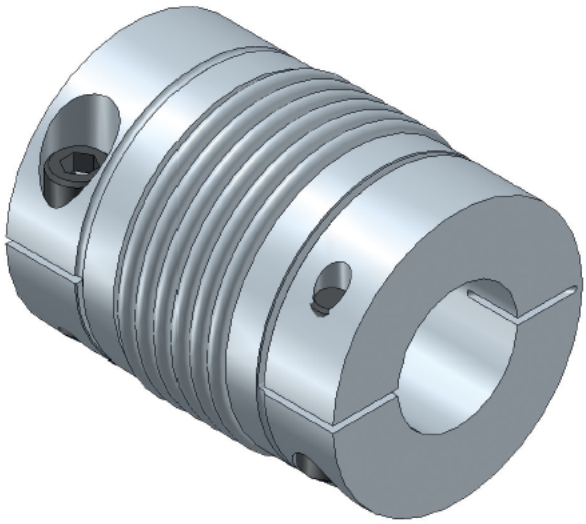

Figure 4.11: WK4 300 bellow coupling by STS Coupling

With the axial connection defined, the casing that protects external components from possible damage (due to the high kinetic energy associated with rotating machinery) can subsequently be designed. Using the dimensions provided by AVL of the prime mover interface as well as the computer-aided design (CAD) model of the EM provided by Dayco, the casing is designed in such a way as to accommodate for both sizes of couplings, namely in the radial direction. Furthermore, its axial length has been selected on the basis of the flange design, EM rotor length and coupling length. To facilitate ease of access of the coupling, two slots are incorporated into the side of the casing. They allow for the tightening of the bolts that ultimately generate the friction necessary to maintain the connection between the two shafts. These features are visible in 4.12.

Finally, the flange design has been performed with the positions of the threaded

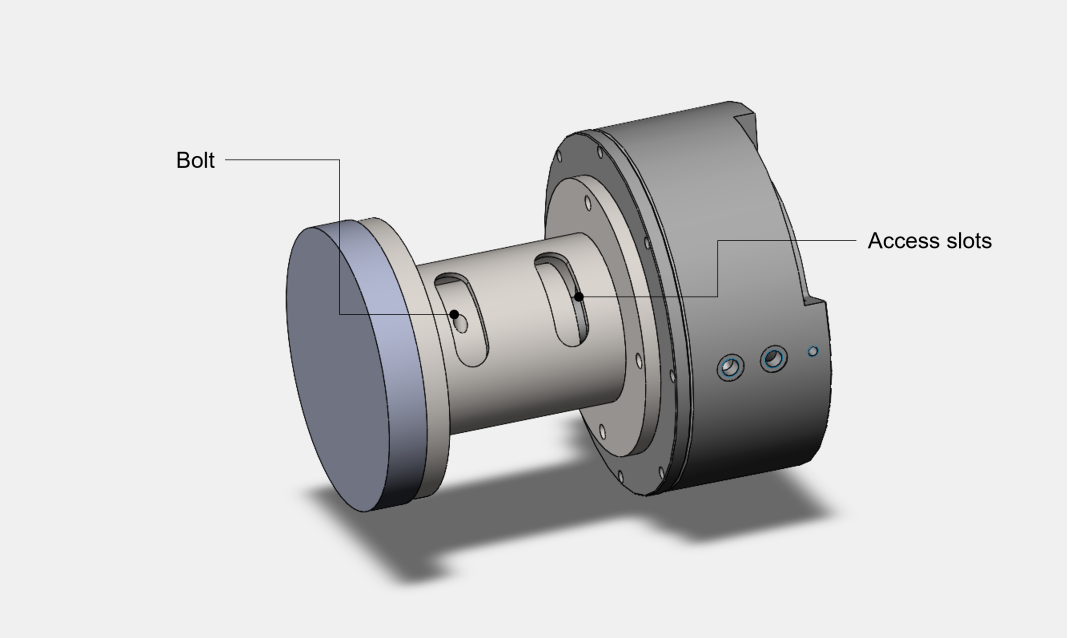

Figure 4.12: Testing assembly

connections and the centering collar considered. A tolerance of H7/h6 has been imposed on the interface of the flange that interacts with the rotor collar of the prime mover, a necessary choice given centering of the rotation axis of the machine with that of the drive unit is necessary. Furthermore, the diameter of the flange shaft (40 mm) has been selected near that of the rotor of the EM (42 mm). This component along with the coupling casing are machined by Dayco and can be seen in a cross section view of the testing assembly in Figure 4.13.

A final consideration is made regarding the physical set-up of the testing assembly, in particular the selection of a supporting platform for the EM. Given that the mass of the machine is 17 kg and its center is at a fixed distance of 0.274 m (L in Figure 4.14) from the surface of the prime mover interface, a resultant moment is generated. The value is roughly 46 Nm, raising the question: will this lead to any damage of the prime mover if the EM is mounted without a supporting platform? Considering the mass of the drive unit is 320 kg and the casing has been roughly over-designed, it can be assumed the unit will be able to support the moment generated by the EM. Therefore the use of such a platform is disregarded in this testing set-up, with the EM connected directly to the prime mover and any axial misalignment is compensated by the WK4 coupling.

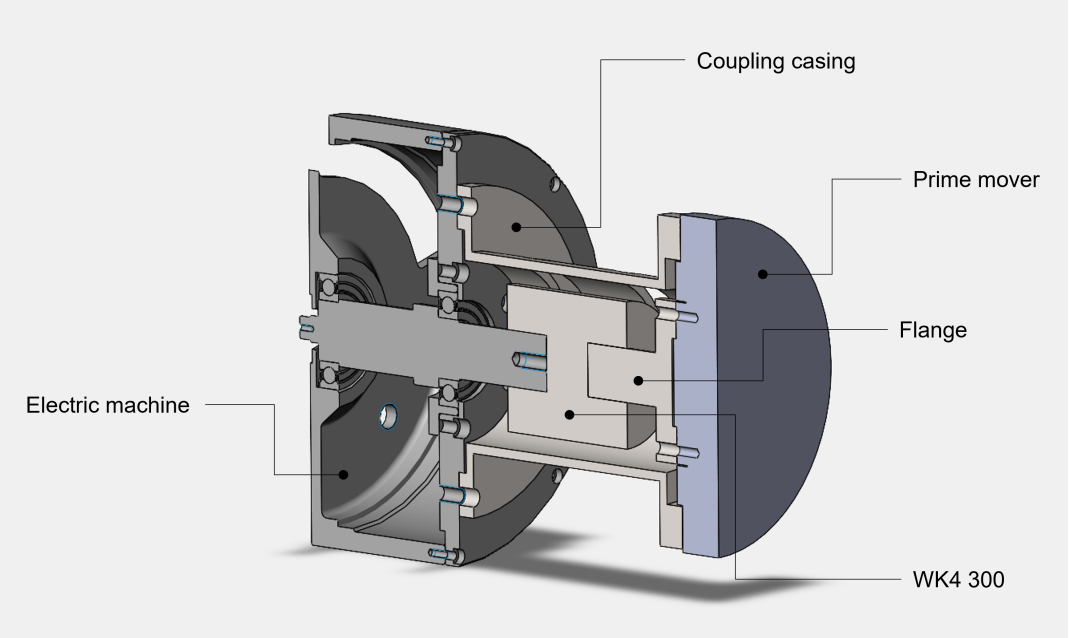

Figure 4.13: Labelled testing assembly of the EM

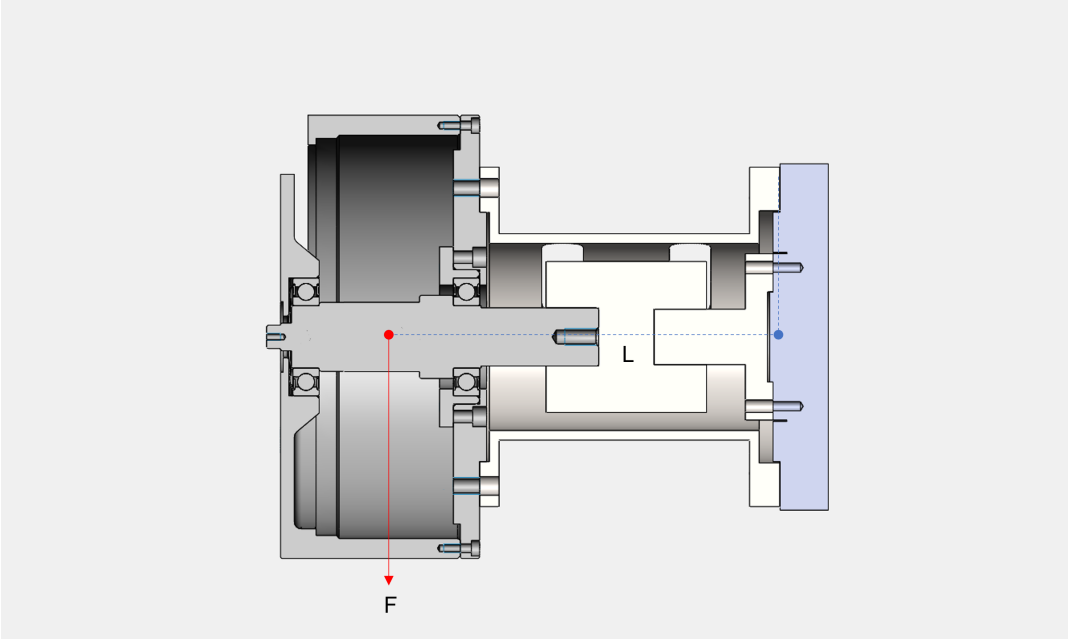

Figure 4.14: EM torque generation with respect to the prime mover

4.1.4 EM mounting

After modelling the assembly, the various components facilitating the connection must be machined. The flange is produced from mild steel and the coupling casing from aluminium due to its larger size. Figure 4.15 displays the WK4 300 coupling, the coupling casing and the flange.

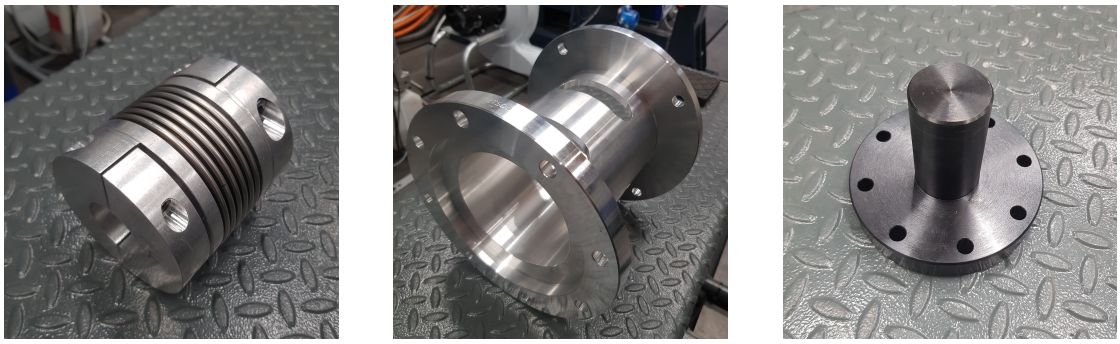

Figure 4.15: Coupling, casing and flange

A factor to be mindful during the early stages of the assembly is the selection of the bolts to secure the static and rotating components to the prime mover. The correct diameters must be selected firstly and then the right lengths should be determined to avoid any interference with internal parts of both machines. The selected bolts for this application are:

1. M12 x 30 for the prime mover side
2. M12 x 25 for the EM side
3. M8 x 35 for the rotor-flange connection

With all the components present, the assembly may be put together following the subsequent steps:

1. Connect the flange to the prime mover interface using the centering collar of the drive unit.
2. Verify the radial deviation of the shaft is in the tenths of a millimeter during the rotation of the flange using a shaft alignment comparator. Figure 4.16 shows the flange connected to the prime mover.
3. Connect the coupling casing to the prime mover and insert the WK4 300 coupling into the shaft of the flange aligning it with the access holes of the casing. Figure 4.17 presents this assembly.

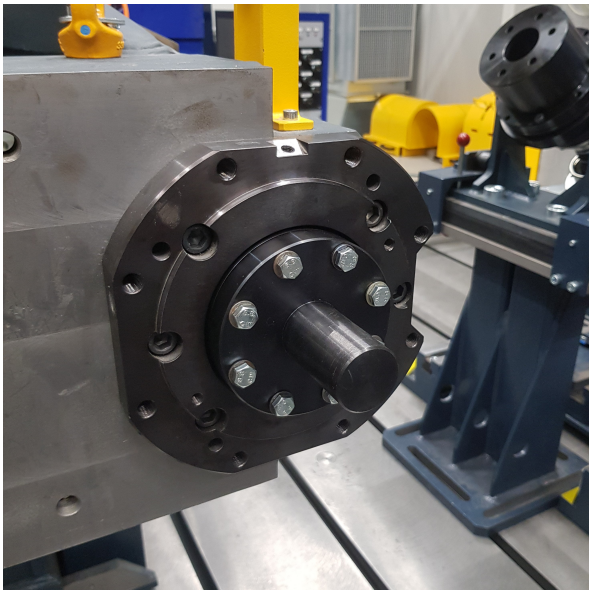

Figure 4.16: Flange-prime mover assembly

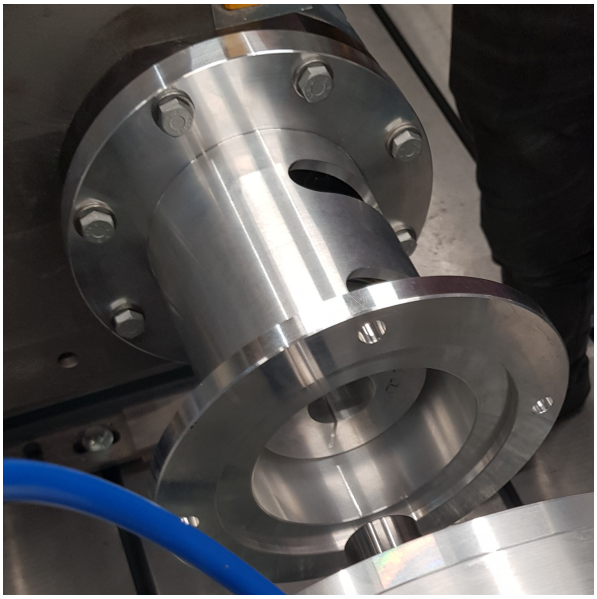

Figure 4.17: Casing-prime mover assembly

4. Connect the EM to the coupling casing ensuring the rotor shaft is inserted into the other end of the coupling.

5. Tighten the bolts on the coupling to secure the connection between the prime mover and EM. Figure 4.18 displays the final mechanical connection between

the EM and prime mover.

Figure 4.18: Mechanical connection

To execute the testing of the EM, certain additional connections need to be made, namely:

1. DC connection from the power distribution unit (PDU) to the inverter that allows for the inverter to draw power from the battery emulator.
2. Three phase current connection from the inverter to the EM.
3. Resolver connection to the inverter by means of a DB15 cable.
4. Temperature sensor connections and 24 V connection (for auxiliary power) between inverter and acquisition unit which directly communicates with the Indicom software acquiring high frequency data.
5. Hydraulic connections from the central system to the inverter and subsequently to the EM. This is done in series typically, with the inverter being cooled first as it has a more stringent cooling requirement compared to the machine.

The AxN-DC.400.6 inverter from Physis (industrial type) is used in this testing procedure. The inverter displays a DC BUS voltage of 800 V and maximum current of 400 A. It is water cooled, with a requested inlet temperature below 20°C, and a

flow rate of 14 liters per minute. As the inverter and the EM are connected in series, the flow rate with respect to the requirement of the machine (6.4 [L/min]) is much larger and the temperature is much lower. This indicates an over-dimensioning of the cooling system for the EM, however should not pose any issues.

Furthermore, a configuration step needs to be performed for the inverter that supplies the three phase current to the machine such that its correct operation is possible. The procedure concerns the current adjustment within an inner loop of the EM control to guarantee the desired torque given the load torque at each time instant. This is done within the inverter, and to guarantee the wide range of torque the machine is required to deliver, the inverter must be calibrated provided with the information of the current, torque and angular speed (or angular position). Typically it is recommended to operate an EM with an inverter produced from the same manufacturer as all these parameters would be known and thus this additional configuration step can be avoided. Figure 4.19 illustrates the full testing set-up, with the hydraulic connections between the inverter, EM and the central system. The DC connection to the inverter is also visible, with only the EM-inverter, EM-acquisition unit and three phase connections between EM and inverter not present as of yet.

Figure 4.19: Experimental assembly

The procedure outlined above concludes the physical testing set-up for the VM EM, allowing for the start of the static test. The procedure includes providing a torque ramp (vector of increasing torque values) for each speed of the machine. This

signal is facilitated, as of the most recent meeting regarding this aspect, through a CAN connection between the control room and the test cell. The issue with this is that the inverter communicates through etherCAT and USB connections, and therefore a decision was made to first commission the inverter through a dedicated software environment provided by Physis through the USB connection. Then the inverter will be modified by changing a hardware component that facilitates a CAN connection, enabling the possibility to communicate to the device through Indicom. These changes will allow to run an automatic routine, covering the entire operating envelope and thus producing the efficiency map.

The VM EM must then be evaluated in its dynamic behaviour, after which the RM EM can be assessed in its entirety from an experimental point-pf-view. This requires additional steps to be followed:

1. Dismount the VM EM from the prime mover by reversing the steps followed for mounting.

2. Disassemble the VM EM by removing the rotor and replace it with the new rotor containing the recycled magnets.

3. Remount the machine onto the prime mover following all the necessary steps presented in this section.

4.2 Dynamic characterisation

4.2.1 Numerical

With the use of the model and its relevant parameters outlined in Chapter 3, the numerical dynamic characterisation may be analysed in this case study. Here, the model is run to obtain the fuel consumption of the system using the baseline ECMS and the Developed ECMS to ultimately obtain the CO_2 emissions comparison. The efficiency maps and the torque-speed curves of the Prius HV EM that are generated in the numerical static characterisation are exploited, where the maps are put together to obtain 3D look-up tables as discussed in Chapter 3.

The fuel consumption per 100 km is computed within the plant of the model, using the speed and torque of the ICE at each time instant that are fed to the ICE map. This gives as an output the mass flow rate of fuel that is subsequently transformed into kilograms of fuel. Converting this value to liters by dividing by the density of the fuel and with the use of the distance covered obtained from the instantaneous speed of the vehicle, the fuel consumption per 100 km is calculated.

The following formulation summarises the statements made:

$$\begin{cases} FC_L = \frac{M_{fuel}}{\rho_{gasoline}} \\ FC_{L/100km} = \frac{FC_L}{x_{km}} \cdot 100 \end{cases} \tag{4.2}$$

with FC_L being the fuel consumption in liters, $\rho_{gasoline}$ the density of the fuel, $FC_{L/100km}$ the fuel consumption per 100 km, and x_{km} the instantaneous distance covered.

The CO_2 emissions in [kg/km] are then computed through the following relation:

$$CO_2 = FC_L \cdot 2.64. \tag{4.3}$$

After having run both versions of the ECMS, by keeping the plant model the same (with a temperature feedback present within), the results indicate minimal change in the fuel consumption. By studying the efficiency of the machine across the driving cycle, it is evident why this is the case: its variation is in the order of magnitude of 10^{-1} as can be seen in Table 4.2. This suggests that the temperature range in which the EM operates does not correspond to a large variation of the efficiency values of the 3D map. Moreover the driving cycle requests the same operating points for both ECMS, particularly the torque values are always below the minimum torque speed curve of 120°C, and therefore we do not see the effect of the degradation of the torque. A combination of these factors, along with the EM already being highly efficient, leads to the minimal variation of the final fuel consumption. Table 4.2 reports the results.

ECMS	Fuel consumption [L/100km]	Average EM efficiency [%]
Baseline	6.849	92.2
Developed	6.847	92.5

Table 4.2: Fuel consumption and average EM efficiency in motor mode comparison

The difference of fuel consumption between the two ECMS is 0.002 [L/100km], translating to a saving of **0.05 [g/km]** for the Developed ECMS. Individually, this number holds little significance in emission decrease, but can still contribute to the total emission saving of the vehicle through a combination of additional hardware on board. Even now the value may not add a significant contribution, however there is the potential for it to be increased. Considering the penalty set forth by the EU for each gram of CO_2 per kilometer, the economic benefit for this scenario for each newly registered vehicle is **4.75€**. With a fleet of 5000 vehicles, this would amount to **23750€** saved by the manufacturer. This gives an idea of

how small emission reductions translate to large economic benefits on top of the more important environmental advantages, however small these values are in this study.

Furthermore, an analysis of the SOC may be made regarding both ECMS. Concerning the baseline ECMS, the variation of the SOC is less pronounced as opposed to that of the Developed ECMS as seen in Figure 4.20. This can be explained with the help of the temperature feedback of the EM, where at the beginning of the cycle the temperature is quite low. With that comes a large difference with respect to the reference temperature in Equation 3.25 and therefore the penalty factor is low. This indicates a large usage of the EM when it is cool and subsequently a lower usage when it exceeds the threshold value. With elevated temperatures, the SOC increases due to the lower usage in motoring mode, however with the difference of the SOC increasing, the penalty factor decreases (as there is a large potential charge that can be exploited) even though the temperature is relatively high. The combination of the difference in the machine temperature and SOC variation dictates the amount of usage of the EM in motoring mode. This type of control may be seen as more taxing on the battery compared to the Baseline ECMS, however has the potential to better exploit the EM and prolong its lifetime in terms of thermal stress.

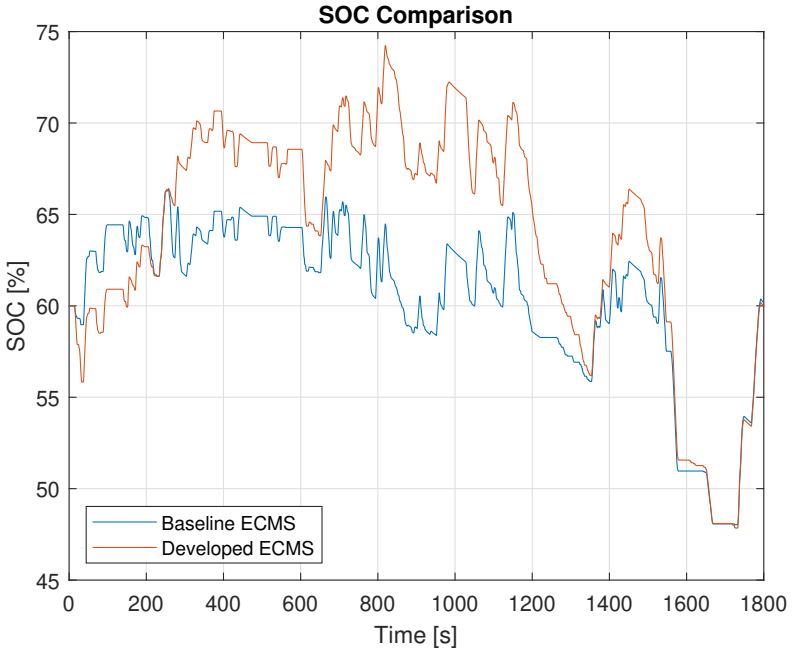

Figure 4.20: SOC comparison

Looking at the temperature variation of the machine in Figure 4.21, one may

notice little change between the two ECMS over the drive cycle. This would be for reasons based on the small efficiency changes described earlier, meaning small differences in power loss at the same time instants and therefore small temperature increment differences. However it may be seen that in some points of operation, the EM temperature difference for the two controllers is noticeable, with the Developed ECMS operating at 1°C lower. This is not a significant number, however indicates that a thermal control of the machine through a controller is possible, and therefore has the potential to be developed further. In addition, the machine is seen to be used more (and therefore has an elevated temperature) in the time range of 1200 to 1400 s when comparing the Developed ECMS to the baseline, a consequence of the controller seeing that the temperature is below the reference value and a large charge being present. Lastly, the correct activation of the coolant is visible as well as the effect the coolant has on the cooling time of the machine. Comparing the decreasing slopes above 90°C and those below, the gradient is observed to be greater for those above as opposed to those below, suggesting a more rapid cooling when the coolant is active.

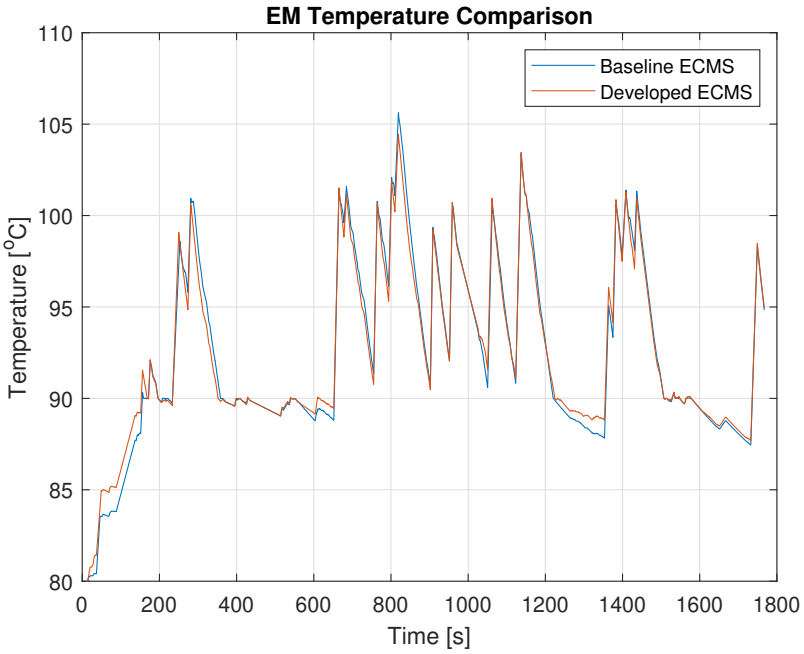

Figure 4.21: Temperature comparison

Certain conclusion can be made concerning the results presented for the numerical dynamic characterisation of the machine at vehicle level. In particular, the Developed ECMS exhibits the potential to exploit the EM to a better degree during the driving cycle, however if the machine used is of poorer efficiency. There must be

a greater decrease of efficiency values across the map to notice a significant change in the fuel consumption of the vehicle. With a fixed torque-speed and efficiency map present in the Baseline ECMS and a three dimensional map varying with temperature present in the Developed ECMS with a temperature feedback which is near to that at which the Baseline map is characterised, it seems that the there is only a small difference between the two controllers during operation. Furthermore, given that the Developed ECMS is able to control the temperature of the EM to some extent, it looks promising for machines outfitted with recycled magnets. EMs with reprocessed magnet material will display lower efficiencies and may be more susceptible to temperature effects, giving a potential utility to the controller that has been developed.

The results of the case study show a strong foundation from which further development can be made, in a way such that fuel consumption savings and temperature mitigation are accentuated. In fact, one such improvement may be to use a genetic algorithm to obtain the various tuneable parameters composing the penalty factor definition, to obtain the optimal set of values that would lead to better results. The limitation observed in this work is the tuning of these parameters manually, and therefore it can be argued that the present solution is not the most optimal, however definitely has the potential to be.

4.2.2 Experimental

Finally, a few words must be dedicated to the experimental dynamic characterisation of the VM EM and the RM EM. This can be done in two ways: either with a **HIL** set-up or by using a **torque profile** generated from an offline dynamic simulation. The latter is less time consuming and less complex, and therefore may be the more appealing strategy. In fact, a model of the type presented in Chapter 3 may be used by running it entirely and extracting the vector of torque values of EM as a response to the WLTP3 cycle. This requires as a prerequisite the torque-speed curves and efficiency maps at various temperatures (for the temperature feedback present), or to have a simpler case, one map at a defined temperature. By using the torque vector, one is able to obtain the efficiency of the machine as it is put under dynamic loads, an important result considering the end-use being a P2 HEV. Furthermore, the experimental set-up presented may be used with no extra hardware required, offering a rapid transition between static and dynamic characterisations.

The HIL set-up requires the use of a real-time communication with the EM connected to the testing facility, where generally speaking, signals from the EM are sent to the model of the vehicle and controller that essentially emulates all the

components that are not present physically. This allows for a cheaper solution in testing not only the component, but also developing the controller when compared to field testing. This is because quick modifications can be made to the controller that would allow for the desired outcome of the system, tuning it in such a way as to exploit the EM to the best of its ability, a similar process to tuning the controller as seen in Chapter 3.

Figure 4.22: HIL set-up

This mode of testing is of importance, allowing one to verify the controller put in place in the numerical model. The tuning of the controller is bound to happen when communicating with the physical EM (whether it being VM or RM based), thus potentially allowing one to quantify the parameter variations with respect to the numerical model. This may prove useful in the future regarding future developments of EMs with recycled magnets embedded, setting a benchmark that can be drawn upon to tune the controller for these newer generations. In any case, the entire physical testing set-up described in this chapter is required to be used in this dynamic testing.

Chapter 5

Conclusions and Future Work

The work presented herein contains a number of conclusions that can be made regarding the topics discussed. Firstly, a primary theme is established: the need for a more sustainable and environmentally-friendly use of raw materials. The continuous use of primary source material for the production of NdFeB magnets for various industrial sectors including the automotive one is unreasonable in the long term, both in an economic sense and sustainability sense. The eVTB project aims to set a stepping stone to solve this problem and avoid the prolonged dependency on another nation for the material and finished product, to promote self-reliance within the European Union. The Politecnico di Torino plays a vital role here, providing the know-how in automotive systems and components as well as their robust testing, both numerically and experimentally. The first part of the work also recapitulates the main electric drives currently present, with the justification of the use of PMSMs for HEV applications. Their operating principles are outlined, forming the basis for the numerical static characterisation performed through finite element analysis. Furthermore, a presentation of various other components that are important for HEV propulsion are discussed, ones that become present in the modelling of the system. The different HEV architecture types are also explained to give an introduction to the layout utilised for this work.

The second part of the activity concerns a state-of-the-art analysis of the viability and potential of recycling NdFeB magnet material, with the outcome being greatly positive. With a large amount of material currently in circulation, studies have shown that a large portion of the future demand can be alleviated through recycling. One of the many current issues is the lack of a standard for recycling and therefore a high cost in doing so, as well as a lack of government incentives. With success in

using recycled magnets in EMs, as well as LCA analyses having been performed that indicate a lower economic and environmental impact, the road towards a more sustainable magnet production is being paved. With the close collaboration between governments, research institutions and industries, recycling of permanent magnets will be solidified as a viable secondary source for the production of EMs and various other components in the near future.

The presentation of control strategies and the model with its controller is made in part 3 of this work. Different HEV control strategies are discussed, with their advantages and disadvantages highlighted to arrive to the ECMS that is used for this study. The model is thoroughly evaluated where it is most necessary due to its complexity, with the addition of a thermal model that estimates the temperature of the EM at each time instant. This model features a variable cooling of the system that prevents excessive charge consumption, with its proper operation seen in Chapter 4. All this has been done to bring the model closer to the real-case scenario. Furthermore, the governing concepts of the Baseline ECMS are explored, as well as the tuning of the necessary parameters present in the adaptive penalty factor formulation by means of a combination of numerical and manual methods. With the degradation of magnet properties seen with increasing operating temperature, a development of the ECMS is proposed by taking into consideration the estimation of the EM temperature. Its tuning is done in the same manner as for the Baseline ECMS.

Finally, the last section of the activity looks at the testing methodology for RM and VM EMs. The presentation of a numerical and experimental route for both the static and dynamic characterisations of each machine is made, one that can be used by an analyst to verify its design and performance. In particular, numerical static characterisation is discussed briefly with a case study on the observation of the results depicting machine performance degradation with elevated temperatures. Furthermore, the mechanical interface design is performed and a guide for EM installation for physical testing concerning all the necessary hydraulic, electrical and mechanical connections is given. Lastly, the numerical dynamic characterisation results of the model presented in part 3 are discussed, showing a close operation of the system between the Baseline ECMS and the Developed ECMS. The potential for the latter is great in the scope of its application to controlling EMs with recycled magnets due to their provisioned lower efficiency and their hypothesised susceptibility to elevated temperatures.

The next steps for this line of work that are to be done include the acquisition of the data to characterise the VM EM statically through the experimental route. The experimental dynamic testing for this machine is also needed to be completed,

with the use of the torque profile as the input. Once the VM EM is fully analysed, the RM EM needs to be evaluated in the same manner regarding the experimental tests. For both cases, the numerical tests are required to be done (static and dynamic) as well. Concerning the control of the vehicle, the immediate next steps are to optimise the tuning of the Developed ECMS through a genetic algorithm. This would aim at obtaining notable differences of performance of the vehicle in terms of fuel consumption, such that the degraded machine (due to the recycled magnets) can be exploited as best as possible. The work that has been done thus far is of importance regarding the preparation for the full characterisation of VM and RM EMs. It has been performed with close collaboration between multiple partners of the project with the common goal of meeting the requirements of the project and engineering novel solutions to combat sustainability issues, ones that will surely be overcome.

Appendix A

Appendix

A.1 Voltage vector

$$\boldsymbol{v_{abc}} = \begin{bmatrix} Vcos\theta_e & Vcos(\theta_e - {}^{2\pi}/_3) & Vcos(\theta_e + {}^{2\pi}/_3) \end{bmatrix}^\top$$

A.2 Current vector

$$\boldsymbol{i_{abc}} = \begin{bmatrix} i_a & i_b & i_c \end{bmatrix}^\top$$

A.3 Inductance matrix

$$L_a = L_1 - L_2 cos(2\theta_e)$$
$$L_b = L_1 - L_2(2\theta_e + {}^{2\pi}/_3)$$
$$L_c = L_1 - L_2(2\theta_e - {}^{2\pi}/_3)$$

$$M_{ab} = -{}^{L_1}/_2 - L_2 cos(2\theta_e - {}^{2\pi}/_3)$$
$$M_{ac} = -{}^{L_1}/_2 - L_2 cos(2\theta_e + {}^{2\pi}/_3)$$
$$M_{bc} = -{}^{L_1}/_2 - L_2 cos(2\theta_e)$$

$$M_{ab} = M_{ba}$$
$$M_{ac} = M_{ca}$$
$$M_{bc} = M_{cb}$$

$$\boldsymbol{L_{abc}} = \begin{bmatrix} L_a & M_{ab} & M_{ac} \\ M_{ba} & L_b & M_{bc} \\ M_{ca} & M_{cb} & L_c \end{bmatrix}$$

A.4 Flux linkage vector

$$\boldsymbol{\lambda_{p,abc}} = \begin{bmatrix} \lambda_p cos\theta_e & \lambda_p cos\theta_e - {}^{2\pi}/_{3}) & \lambda_p cos(\theta_e + {}^{2\pi}/_{3}) \end{bmatrix}^\top$$

A.5 Resistance matrix

$$\boldsymbol{R} = \begin{bmatrix} R & 0 & 0 \\ 0 & R & 0 \\ 0 & 0 & R \end{bmatrix}$$

A.6 Clarke transform matrix

$$\boldsymbol{T_c} = \begin{bmatrix} 1 & {}^{-1}/_{2} & {}^{-1}/_{2} \\ 0 & {}^{\sqrt{3}}/_{2} & {}^{-\sqrt{3}}/_{2} \\ {}^{1}/_{2} & {}^{1}/_{2} & {}^{1}/_{2} \end{bmatrix}$$

A.7 Park transform matrix

$$\boldsymbol{T_p} = \begin{bmatrix} cos\theta_e & sin\theta_e & 0 \\ -sin\theta_e & cos\theta_e & 0 \\ 0 & 0 & 1 \end{bmatrix}$$

A.8 Park-Clarke transform matrix

$$\boldsymbol{T_{pc}} = \frac{2}{3} \begin{bmatrix} cos\theta_e & sin(\theta_e - {}^{2\pi}/_{3}) & cos(\theta_e + {}^{2\pi}/_{3}) \\ -sin\theta_e & -sin(\theta_e - {}^{2\pi}/_{3}) & -sin(\theta_e + {}^{2\pi}/_{3}) \\ {}^{1}/_{2} & {}^{1}/_{2} & {}^{1}/_{2} \end{bmatrix}$$

Bibliography

[1] K.V. Singh, H.O. Bansal, and D. Singh. «A comprehensive review on hybrid electric vehicles: architectures and components». In: *Journal of Modern Transportation* 27 (Mar. 2019), pp. 77–107 (cit. on pp. 3, 5, 13, 15, 18).

[2] European Commission. *CO_2 emission performance standards for cars and vans*. URL: `https://ec.europa.eu/clima/eu-action/transport-emissions/road-transport-reducing-co2-emissions-vehicles/co2-emission-performance-standards-cars-and-vans_en` (visited on 09/04/2022) (cit. on p. 4).

[3] A. Karki et al. «Status of Pure Electric Vehicle Power Train Technology and Future Prospects». In: *Applied System Innovation* 3 (Aug. 2020) (cit. on pp. 5, 6).

[4] A. Khaligh and Z. Li. «Battery, Ultracapacitor, Fuel Cell, and Hybrid Energy Storage Systems for Electric, Hybrid Electric, Fuel Cell, and Plug-In Hybrid Electric Vehicles: State of the Art». In: *IEEE Transactions on Vehicular Technology* 59 (July 2010) (cit. on p. 13).

[5] M. Ehsani, K.V. Singh, and R.T. Mehrjardi. «State of the Art and Trends in Electric and Hybrid Electric Vehicles». In: *Proceedings of the IEEE* 109 (June 2021) (cit. on p. 14).

[6] X-engineer. *Types of Mild Hybrid Electric Vehicles (MHEV)*. URL: `https://x-engineer.org/mild-hybrid-electric-vehicles-mhev-types/` (visited on 08/25/2022) (cit. on p. 15).

[7] W. Schoffmann et al. «The tailored powertrain for 48 V – options for the gasoline engine – chance for future Diesel engines». In: *4th International Engine Congress - Meeting Place for the Engine Community*. Graz, Austria, 2017, pp. 261–296 (cit. on p. 16).

[8] D. Prosperi et al. «Performance comparison of motors fitted with magnet-to-magnet recycled or conventionally manufactured sintered NdFeB». In: *Journal of Magnetism and Magnetic Materials* 460 (Apr. 2018) (cit. on pp. 19, 26, 27).

[9] C. Jonsson et al. «The extraction of NdFeB magnets from automotive scrap rotors using hydrogen». In: *Journal of Cleaner Production* 277 (Sept. 2020) (cit. on pp. 20, 25).

[10] D. Guyonnet et al. «Material flow analysis applied to rare earth elements in Europe». In: *Journal of Cleaner Production* 107 (Sept. 2015), pp. 215–228 (cit. on p. 20).

[11] K. Habib and H. Wenzel. «Exploring rare earths supply constraints for the emerging clean energy technologies and the role of recycling». In: *Journal of Cleaner Production* 84 (Apr. 2014), pp. 348–359 (cit. on p. 21).

[12] D. Schuler et al. *Final Report for The Greens/EFA Group in the European Parliament*. Tech. rep. Darmstadt, Germany: Oko-institut, 2011 (cit. on p. 21).

[13] Y. Yang et al. «REE Recovery from End-of-Life NdFeB Permanent Magnet Scrap: A Critical Review». In: *Journal of Sustainable Metallurgy* 3 (Sept. 2016), pp. 122–149 (cit. on p. 22).

[14] Rita. Schulze and M. Buchert. «Estimates of global REE recycling potentials from NdFeB magnet material». In: *Resources, Conservation and Recycling* 3 (June 2016), pp. 12–27 (cit. on p. 22).

[15] Z. Li et al. «Direct reuse strategies of rare earth permanent magnets for PM electrical machines – an overview study». In: *The European Physical Journal: Applied Physics* 86 (Apr. 2019) (cit. on p. 23).

[16] A. Walton et al. «The use of hydrogen to separate and recycle neodymium-iron-boron-type magnets from electronic waste». In: *Journal of Cleaner Production* 104 (May 2015) (cit. on p. 24).

[17] H. Jin et al. «Comparative Life Cycle Assessment of NdFeB Magnets: Virgin Production versus Magnet-to Magnet Recycling». In: *Procedia CIRP*. Vol. 48. 2016, pp. 45–50 (cit. on pp. 25, 26).

[18] Q. Xue et al. «A Comprehensive Review on Classification, Energy Management Strategy, and Control Algorithm for Hybrid Electric Vehicles». In: *Energies* 13 (Oct. 2020) (cit. on p. 30).

[19] S. Hegde et al. «Optimal Selection of Equivalence Factors for ECMS in Mild Hybrid Electric Vehicles». In: *Proceedings of the ASME 2021 INternational Design Engineering Technical Conferences and Computers and Information in Engineering Conference*. 2021 (cit. on pp. 39, 43, 44).

[20] X. Liu, D. Qin, and S. Wang. «Minimum Energy Management Strategy of Equivalent Fuel Consumption of Hybrid Electric Vehicle Based on Improved Global Optimization Equivalent Factor». In: *Energies* 12 (May 2019) (cit. on p. 42).